THE JOURNAL OF PHYSICAL CHEMISTRY A
A JOURNAL OF THE AMERICAN CHEMICAL SOCIETY

pubs.acs.org/JPCA

Article

# Tracking Isomerizations of High-Energy Adenine Cation Radicals by UV−Vis Action Spectroscopy and Cyclic Ion Mobility Mass Spectrometry

Václav Zima,[‖] Mikuláš Vlk,[‖] Jiahao Wan, Josef Cvačka, and František Tureček*

Cite This: *J. Phys. Chem. A* 2023, 127, 5899−5913

Read Online

ACCESS | Metrics & More | Article Recommendations | Supporting Information

**ABSTRACT:** We report experimental and computational studies of protonated adenine C-8 $\sigma$-radicals that are presumed yet elusive reactive intermediates of oxidative damage to nucleic acids. The radicals were generated in the gas phase by the collision-induced dissociation of C-8−Br and C-8−I bonds in protonated 8-bromo- and 8-iodoadenine as well as by 8-bromo- and 8-iodo-9-methyladenine. Protonation by electrospray of 8-bromo- and 8-iodoadenine was shown by cyclic-ion mobility mass spectrometry (c-IMS) to form the N-1-H, N-9-H and N-3-H, N-7-H protomers in 85:15 and 81:19 ratios, respectively, in accordance with the equilibrium populations of these protomers in water-solvated ions that were calculated by density functional theory (DFT). Protonation of 8-halogenated 9-methyladenines yielded single N-1-H protomers, which was consistent with their thermodynamic stability. The radicals produced from the 8-bromo and 8-iodo adenine cations were characterized by UV−vis photodissociation action spectroscopy (UVPD) and c-IMS. UVPD revealed the formation of C-8 $\sigma$-radicals along with N-3-H, N-7-H-adenine $\pi$-radicals that arose as secondary products by hydrogen atom migrations. The isomers were identified by matching their action spectra against the calculated vibronic absorption spectra. Deuterium isotope effects were found to slow the isomerization and increase the population of C-8 $\sigma$-radicals. The adenine cation radicals were separated by c-IMS and identified by their collision cross sections, which were measured relative to the canonical N-9-H adenine cation radical that was cogenerated in situ as an internal standard. Ab initio CCSD(T)/CBS calculations of isomer energies showed that the adenine C-8 $\sigma$-radicals were local energy minima with relative energies at 76−79 kJ mol$^{-1}$ above that of the canonical adenine cation radical. Rice−Ramsperger−Kassel−Marcus calculations of unimolecular rate constants for hydrogen and deuterium migrations resulting in exergonic isomerizations showed kinetic shifts of 10−17 kJ mol$^{-1}$, stabilizing the C-8 $\sigma$-radicals. C-8 $\sigma$-radicals derived from N-1-protonated 9-methyladenine were also thermodynamically unstable and readily isomerized upon formation.

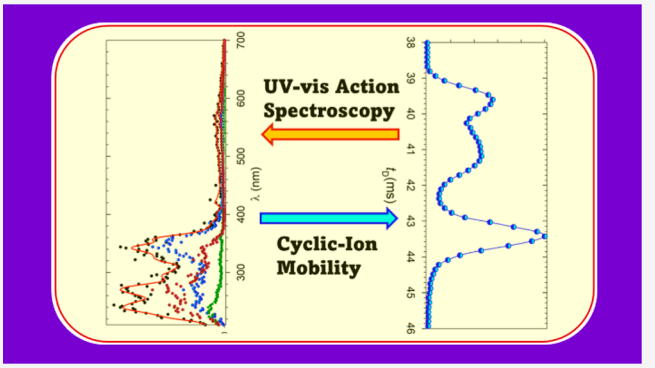




## INTRODUCTION

C-8 is the most common site of chemical modifications of purine nucleobases caused by reactive oxidative species or electrophiles. Hydroxyl radical attack proceeds predominantly at C-8 in guanine where it is associated with the formation of cation radicals, resulting in oxidation and the formation of 8-oxoguanine lesions.[1] Halogenation at adenine C-8 in nucleosides and nucleotides has been utilized for DNA and RNA modifications[2−5] and is also known to proceed enzymatically.[6−8] Nucleobase ionization, which primarily affects the $\pi$-electron system in the cation radicals, can initiate downstream chemical reactions affecting C-8.[1,9−15] However, the detection and isolation of nucleobase cation radicals are made difficult by their high proclivity for fast proton transfer to the surrounding medium.[16−21] Recently, nucleobase, nucleoside, and oligonucleotide cation radicals have been generated in the rarefied gas phase, where they can be isolated by mass and studied spectroscopically. There are currently four general methods of making DNA-related cation radicals, as shown in Scheme 1. Collision-induced electron transfer in gas-phase ternary copper complexes[22,23] has been shown first by O'Hair and co-workers to form cation radicals of DNA nucleobases[24,25] and has also been used to generate cation radicals of unnatural, hachimoji,[26] bases (reaction 1 in Scheme 1).[27,28] This method is limited to nucleobases and readily oxidizable 2′-deoxyguanosine, guanosine, and their derivatives.[24] With adenosine, cytidine, and thymidine ribo and 2′-deoxyribonucleosides, collisional

Received: May 15, 2023
Revised: June 27, 2023
Published: July 11, 2023

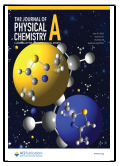

**Scheme 1. Gas-Phase Reactions Yielding Adenine Cation Radicals**

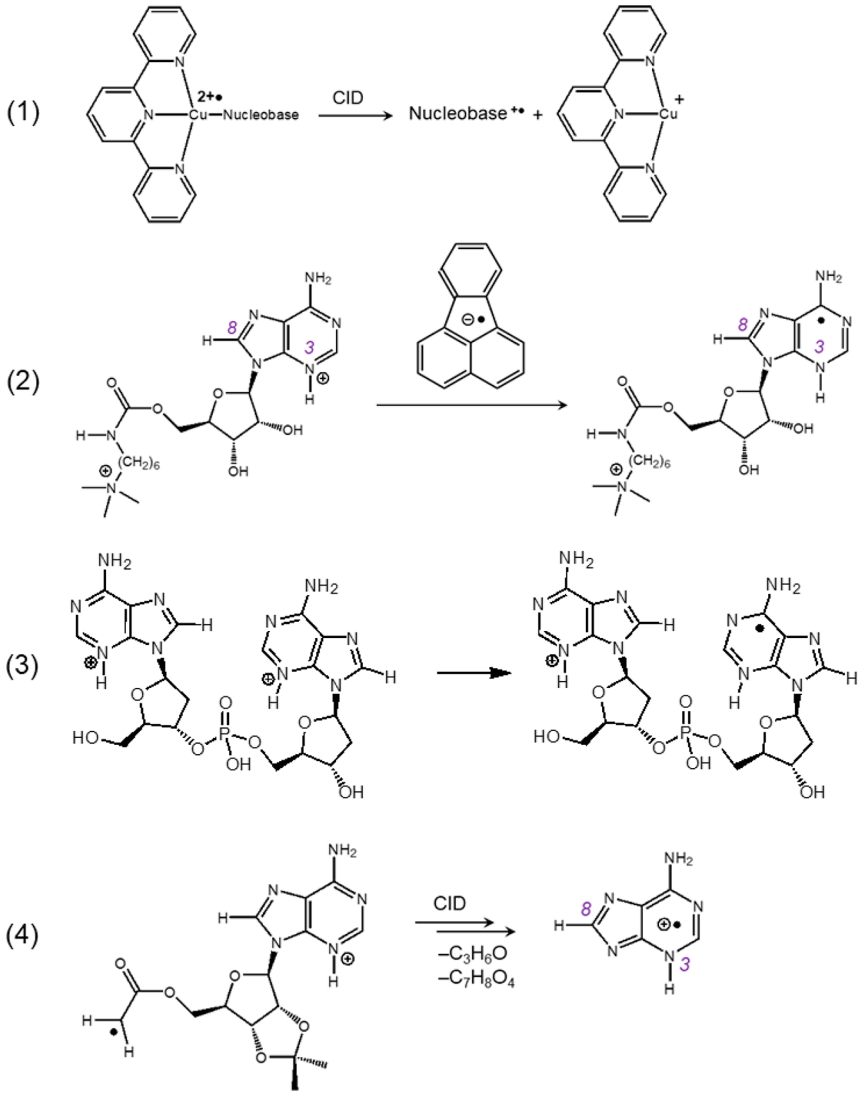


**Scheme 2. Generation of Adenine C-8 Cation Radicals**

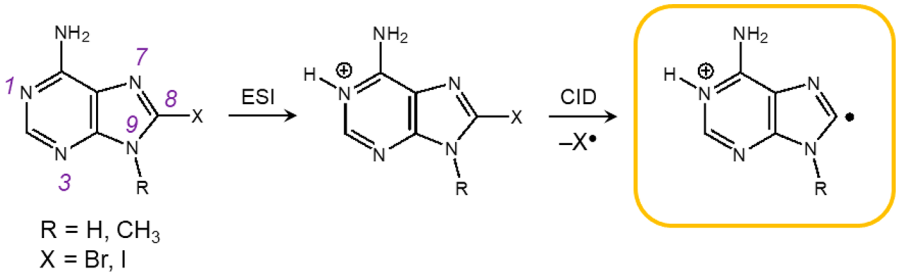


activation of ternary copper complexes results in glycosidic bond dissociation rather than electron transfer.[24,29] Electron transfer to doubly charged nucleoside ions that were furnished with a fixed-charge group has been shown to result in the reduction of the charged nucleobase, producing adenosine, guanosine, and cytidine radicals, as shown for adenosine in reaction 2 (Scheme 1).[30] A similar approach employing electron transfer reduction has been developed to generate cation radicals of dinucleotides,[31] DNA codon trinucleotides,[32] and tetranucleotides (reaction 3, Scheme 1).[33] Finally, we have shown recently that upon collisional activation, nucleosides equipped with a radical initiator group at O-5′ undergo a cascade breakup of the ribose ring, forming unusual adenine and guanine cation-radical tautomers, as shown for adenine in reaction 4 (Scheme 1).[34] A common feature of reactions 1−4 has been that they produced cation radicals that had the electron vacancy delocalized over the nucleobase $\pi$-electron system. However, guanine and 9-methylguanine cation radicals generated by reaction 1 have been shown to undergo ion−molecule reactions with water, resulting in hydrogen transfer and hydroxylation at C-8.[12,13,15] Clearly, an approach to



https://doi.org/10.1021/acs.jpca.3c03179
J. Phys. Chem. A 2023, 127, 5899−5913

generate charged purine C-8 radicals is needed in order to investigate their intrinsic properties by spectroscopic methods.

Aromatic and heteroaromatic $\sigma$-radicals have been previously generated in the gas phase, according to two methods. Kenttamaa and co-workers used the collision-induced dissociation (CID) of even-electron quinoline cations furnished with substituents, such as the nitro group or iodine, that were eliminated as radicals, forming $\sigma$-radical ions that were characterized by ion−molecule reactions.[35−38] Julian and co-workers have used the photodissociation of iodotyrosine formed in situ in peptides to generate tyrosyl $\sigma$-radicals that have been shown to undergo intramolecular hydrogen-transfer reactions.[39−41] Here, we implement the collision-activation method to generate charged adenine C-8 $\sigma$-radicals by the homolytic cleavage of C−Br and C−I bonds in 8-bromo and 8-iodoadenine and related 9-methyladenine cations (Scheme 2).

The dissociation energy of the C−Br bond in 8-bromoadenine has been calculated as 346 kJ mol$^{-1}$,[42] representing a moderately strong bond. The aromatic C(sp$^2$)−I bond in iodobenzene has been estimated to be about 70 kJ mol$^{-1}$ weaker than the C(sp$^2$)−Br bond in bromobenzene,[43] and a similar C−I bond weakening to BDE $\approx$ 276 kJ mol$^{-1}$ can be expected for 8-iodoadenine cations. Both the C−Br and C−I bond dissociation energies are within the range achievable by CID in tandem mass spectrometry.

To characterize the adenine cation radicals formed, we used UV−vis photodissociation action spectroscopy (UVPD).[44,45] This method relies on the photodissociation of mass-selected ions, whereby the wavelength-dependent formation of photoproduct ions is used to retrieve the absorption profile of the precursor ion. UVPD has been shown to differentiate gas-phase ion isomers,[46,47] including nucleobase cation radicals, such as adenine,[48] guanine,[49] cytosine,[50] and thymine.[51] In addition to spectroscopic characterization, we apply cyclic ion mobility mass spectrometry (c-IMS)[52] to separate isomers and characterize them by their collision cross sections (CCS). This includes a new approach to c-IMS whereby we use near-$m/z$ matching of diverse ion precursors for the internal calibration of arrival times of transient species generated by CID. While ion mobility measurements of CCS have become widespread,[53] to our knowledge there have been only a few studies that addressed cation radicals.[54,55] Ion mobility in combination with photodissociation and photoisomerization has been pioneered by Bieske and co-workers to resolve and characterize ion tautomers.[56,57] We combine the experimental results from UV−vis action spectroscopy and c-IMS with theoretical calculations of ion structures, vibronic absorption spectra, collision cross sections, and isomerization energetics and kinetics to assign structures to adenine cation radicals and track their isomerization in the gas phase.

## EXPERIMENTAL SECTION

**Materials and Methods.** 8-Bromodoadenine, 8-iodoadenine, 8-bromo-9-methyladenine, and 8-iodo-9-methyladenine were synthesized using standard methods and characterized by NMR spectroscopy and mass spectrometry. Synthetic details, references, and NMR spectra are described in the Supporting Information (Schemes S1−S3 and Figures S2−S14). CID tandem mass spectrometry was performed on a Bruker amaZon 3D ion trap mass spectrometer (Bruker Daltonik, GmbH, Bremen, Germany) at excitation amplitudes, allowing dissociation. UV−vis action spectra were obtained using an EKSPLA NL301G laser (Altos Photonics, Bozeman, MT, USA). A beam of photon pulses at a 20 Hz frequency and a 3 to 6 ns pulse width was directed into a PG142C unit (Altos Photonics, Bozeman, MT, USA) which incorporated a third-harmonic generator and an optical parametric oscillator (OPO) coupled with an optional second-harmonic generator to enable wavelength tuning between 210 and 700 nm.[58] The laser beam (6 mm diameter) exiting the PG142C unit was aligned and focused into the ion trap of the modified mass spectrometer by a series of mirrors, optical posts, and telescopic lenses (Thorlabs, Newton, NJ, USA) to achieve the photodissociation of isolated ions. A fast steering mirror (Newport Corporation, Irvine, CA, USA) was implemented in the optical setup to improve beam alignment and ultraviolet photodissociation (UVPD) reproducibility. The laser pulse energies, typically ranging from 0.2 to 4.0 mJ, were measured at each experimental UVPD wavelength using an EnergyMax-USB J-10MBenergy sensor (Coherent Inc., Santa Clara, CA, USA) to calibrate the action spectra. The OPO was scanned in three regions: 210−354, 355−409, and 410−700 nm. Ion mobility was measured on a SELECT SERIES cyclic ion mobility spectrometer (c-IMS) (Waters Corp., Wilmslow, U.K.).[52] Samples were introduced by a nanoelectrospray ion source using in-house-pulled capillaries. A 5 $\mu$L portion of the sample was introduced into a borosilicate capillary with an orifice diameter of ~1 $\mu$m pulled on a P1000 capillary puller (Sutter Instrument, Novato, USA). A spray voltage of ~1 kV was applied using a stainless steel filament inserted into the capillary. The cone voltage was set to 40 V with a source offset of 10 V, source temperature of 40 °C, step wave body gradient of 20 V, head gradient of 10 V, trap DC bias of 35 V, and transfer CE of 4 V. Selection of the precursor ion was done by setting up the quadrupole isolation as follows: high mass 15, low mass 18. Fragmentation prior to IMS was performed in the trap region of the instrument. For successful transport of labile ions throughout the ion optics to the detector, specifically fragment ions at $m/z$ 135 and 149, several instrumental parameters had to be adjusted: trap TW pulse height 1 V, post-trap gradient 7 V, step wave RF 150 V, ion guide RF 300 V, trap RF 250 V, drift cell RF 100 V, transfer RF 200 V, and transfer RF gain 5. Collision energies for the generation of fragment ions at $m/z$ 135 and 149 were 35 eV for halogenated adenine ions and 2 × 20 eV for the [Cu-terpy-adenine]$^{2+\bullet}$ complexes. The parameters for the IMS were set as follows: helium flow rate 120 mL/min, nitrogen flow rate 40 mL/min, array offset 70 V, racetrack bias 70 V, and traveling wave (TW) velocity 900 m/s. The TW height was set to 30 and 20 V for precursor and fragment ion separation, respectively. Ion mobility separation of precursor ions was achieved in a multipass experiment at TW velocity 900 m/s and TW height 30 V. The IMS experiment sequence consisted of injection, separation, and ejection steps, while the parameters of the first and last step were kept constant. The separation time was adjusted based on the number of passes. The same method was used for the separation of fragment ions at $m/z$ 135 and 149 except that the TW height was set to 20 V. Fragment ions were separated in one, two, and three passes. A gradual decrease in signal intensity with an increasing number of passes was observed, suggesting a limited stability of the cation-radical species. Calibration details for multipass ion arrival times and collision cross sections data are given in the Supporting Information (Tables S1 and S2 and Figure S1).

**Calculations.** Standard ab initio and density functional theory calculations were performed using the *Gaussian 16*



https://doi.org/10.1021/acs.jpca.3c03179
J. Phys. Chem. A 2023, 127, 5899−5913

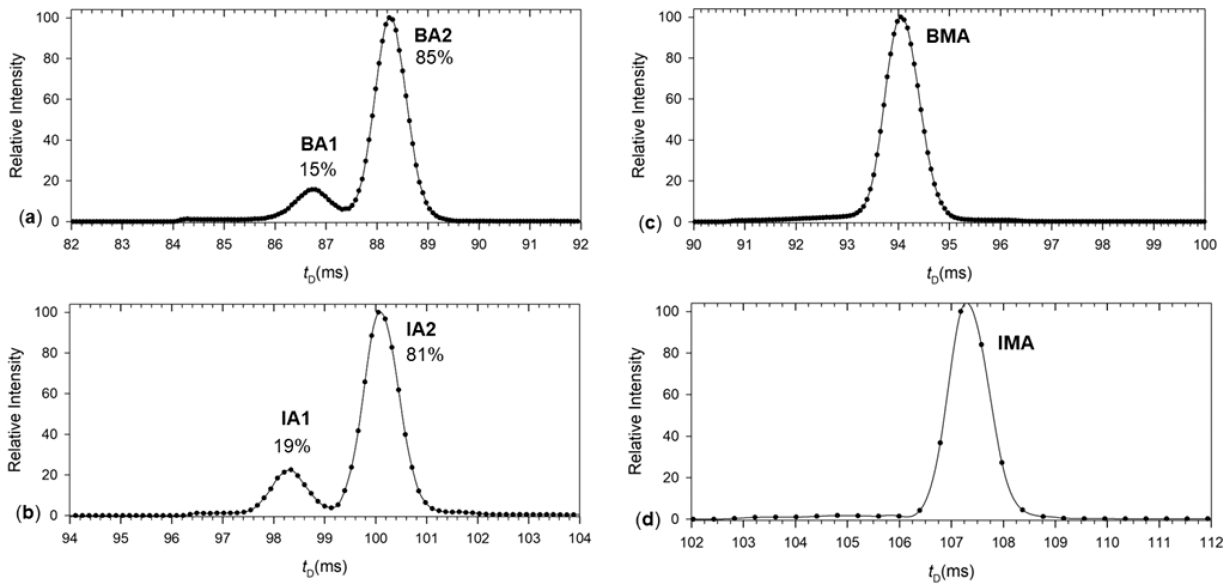


**Figure 1.** Arrival time distributions after (a) 15 passes in c-IMS of 8-bromoadenine cation monitored at $m/z$ 213.9701 ($C_5H_5N_5{}^{79}Br^+$); (b) 16 passes in c-IMS of 8-iodoadenine cation monitored at $m/z$ 261.9576 ($C_5H_5N_5I^+$); (c) 15 passes in c-IMS of 8-bromo-9-methyladenine cation monitored at $m/z$ 227.9880; and (d) 15 passes in c-IMS of 8-iodo-9-methyladenine cation monitored at $m/z$ 275.9761. Fifteen passes corresponded to a 14.7 m ion trajectory path length in c-IMS.

program (revision B.01) that was licensed from Gaussian, Inc. (Wallingford, CT). Structures were optimized with B3LYP[59] and M06-2X[60] with the 6-31+G(d,p) basis set and reoptimized with M06-2X/6-311++G(2d,p). Local energy minima and transition states were characterized by B3LYP harmonic frequency calculations. All calculations of open-shell systems were performed in the spin-unrestricted formalism. The optimized structures were used to calculate single-point energies with Møller–Plesset theory[61] calculations using frozen core excitations (MP2(fc)) and the correlation-consistent aug-cc-pVDZ, aug-cc-pVTZ, and aug-cc-pVQZ basis sets.[62] The MP2 and Hartree–Fock energies were used to fit the $E_{corr} = a + bX^{-3}$ function,[63,64] where $X$ is the $\zeta$ split in the correlation-consistent basis set. The fitted parameter $a$ provided an estimate of the MP2 correlation energy at the complete basis set (CBS) limit, $E_{corr,CBS}$, for $X \rightarrow \infty$. This was further combined with coupled cluster calculations[65] including single, double, and disconnected triple excitations,[66] CCSD-(T)/aug-cc-pVDZ, to estimate correlated energies at the CBS according to the formula

$$E[\text{CCSD(T)/CBS}] \approx E[\text{CCSD(T)/aug-cc-pVDZ}] - E[\text{MP2/aug-cc-pVDZ} + E[\text{HF/aug-cc-pVQZ}] + E_{corr,CBS}$$

Excited electronic states were calculated using time-dependent DFT[67] with the M06-2X/6-31+G(d,p) basis set. Previous benchmarking of M06-2X/6-31+G(d,p) TD-DFT excitation energies of nucleobase cation radicals against those calculated with equation-of-motion CCSD/6-31+G(d,p) has shown close correspondence of both data sets.[27] Vibronic absorption spectra were calculated for TD-DFT excitations from 300 Wigner configurations[68,69] that were generated from normal modes at 310–350 K, which simulated the ion temperature in the ion trap. Typically, 20–25 excited electronic states were included in each calculation to cover the experimental wavelength range below 200 nm. These calculations used the Newton X program.[70] Collision cross sections in nitrogen were calculated by the ion trajectory (IT) method using MobCal[71] and the M06-2X/6-31+G(d,p) optimized geometries and atomic charge densities. Ion trajectory parameters for bromine and iodine were obtained from the code of Kim and co-workers[72,73] and incorporated into the MobCal Fortran code. Rice–Ramsperger–Marcus–Kassel (RRKM) calculations were carried out using the QCEP program[74] that was recompiled and run under Windows.[75]

## RESULTS AND DISCUSSION

**Ion Formation.** Precursor ions were generated by electrospray ionization of 8-bromoadenine and 8-iodoadenine and characterized by c-IMS and CID-MS$^2$. According to previous studies, adenine protonation has been presumed to chiefly produce the N-1-H, N-9-H protomer,[76] although the N-3-H, N-7-H protomer has been calculated to be only a few kJ mol$^{-1}$ thermodynamically less stable.[77−79] By analogy, electrospray protonation of 8-bromoadenine and 8-iodoadenine could produce the corresponding N-1-H, N-9-H and N-3-H, N-7-H protomers. We addressed this question by c-IMS that showed two peaks for both $(C_5H_4N_5Br + H)^+$ from bromoadenine (**BA1**$^+$, **BA2**$^+$) and $(C_5H_4N_5I + H)^+$ from 8-iodoadenine (**IA1**$^+$, **IA2**$^+$) (Figure 1a,b). The major components at longer arrival times represented 85 and 81% for **BA2**$^+$ and **IA2**$^+$, respectively, based on the peak integrated intensities. The components were assigned on the basis of calculated isomer equilibrium concentrations and relative collision cross sections. The optimized structures showed the N-3-H, N-7-H isomer (**BA1**$^+$) to have a Gibbs energy 310 K higher than that of the N-1-H, N-9-H isomer (**BA2**$^+$), indicating a lower equilibrium concentration of the former in the mixture. The difference, $\Delta G_{310} = G_{310}(\mathbf{BA1}^+) - G_{310}(\mathbf{BA2}^+)$ that was calculated with M06-2X/aug-cc-pVTZ increased from 0.4 kJ mol$^{-1}$ for gas-phase ions to 4 kJ mol$^{-1}$ when solvation was included in water. The latter $\Delta G_{310}$ gave a predicted 18:82 ratio of **BA1**$^+$:**BA2**$^+$ which was close to the integrated ATD peak intensities. Similarly, the $\Delta G_{310}$ =


https://doi.org/10.1021/acs.jpca.3c03179
J. Phys. Chem. A 2023, 127, 5899−5913

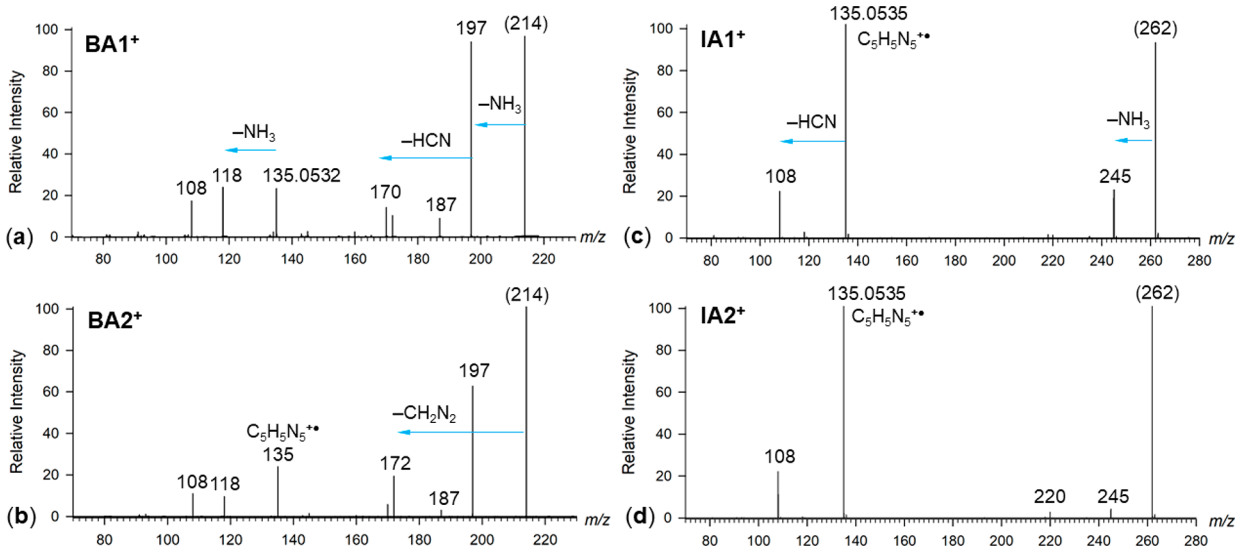


**Figure 2.** CID-MS$^2$ spectra of c-IMS separated (a, b) 8-bromoadenine ions and (c, d) 8-iodoadenine ions.

$G_{310}(\mathbf{IA1}^+) - G_{310}(\mathbf{IA2}^+)$ = 5.5 kJ mol$^{-1}$ value that was calculated for solvated 8-iodoadenine ions indicated an 11:89 ratio for $\mathbf{IA1}^+$ and $\mathbf{IA2}^+$ at equilibrium, which was consistent with the integrated intensities of the ATD peaks. It should be noted that the calculated Gibbs energy differences were small and possibly within the uncertainty limits of DFT calculations. This was checked with CCSD(T)/CBS calculations of adenine N-1-H, N-9-H and N-3-H, N-7-H $(C_5H_5N_5 + H)^+$ ion protomers that favored the former by $\Delta G_{310}$ = −3.5 kJ mol$^{-1}$ for the solvated ions, to be compared with the M06-2X/aug-cc-pVTZ result ($\Delta G_{310}$ = −3.0 kJ mol$^{-1}$). This benchmarking and the Gibbs-energy consistency for 8-bromoadenine and 8-iodoadenine ions appeared to give credit to the DFT accuracy.

Another criterion for structure assignment was the experimental and calculated collision cross sections (CCS). The measured CCS of $\mathbf{BA1}^+$ and $\mathbf{BA2}^+$, 136.6 and 137.4 Å$^2$, respectively, were matched against the calculated CCS of the N-3-H, N-7-H and N-1-H, N-9-H $(C_5H_4N_5Br + H)^+$ protomers at 134.7 and 136.6 Å$^2$, respectively. Rather than an absolute match between the experimental and calculated CCS, which was within 1.4 and 0.6% for the isomers, we considered the relative CCS that assigned the N-3-H, N-7-H protomer to $\mathbf{BA1}^+$ and the N-1-H, N-9-H protomer to $\mathbf{BA2}^+$. Similar results were obtained for $(C_5H_4N_5I + H)^+$ from 8-iodoadenine, where the experimental CCS of $\mathbf{IA1}^+$ and $\mathbf{IA2}^+$, 139.0 and 139.7 Å$^2$, respectively, were aligned with the N-3-H, N-7-H and N-1-H, N-9-H protomers with the calculated CCS of 140.7 and 144.2 Å$^2$, respectively. Hence, the combined Gibbs energy and ion mobility data were consistent in assigning the major components to the N-1-H, N-9-H protomeric forms for both $(C_5H_4N_5Br + H)^+$ and $(C_5H_4N_5I + H)^+$ ions. We note that a recent study that used the combination of differential ion mobility and action spectroscopy of protonated adenine has identified a minor N-3-H protomer eluting before the major N-1-H protomer,[80] which was consistent with our conclusions regarding the 8-halogenated adenine ions.

The arrival-time distributions of $(C_6H_6N_5Br + H)^+$ ions from 8-bromo-9-methyladenine (**BMA**) and $(C_6H_6N_5I + H)^+$ ions from 8-iodo-9-methyladenine (**IMA**) ions showed essentially single peaks, each amounting to >98% of the ion current. This was consistent with the ion thermochemistry that favored the formation of 99 and 99.8% N-1-H protonated tautomers of 9-methyladenine[81] and 8-bromo-9-methyladenine, respectively, according to calculated Gibbs energies of water-solvated ions. A similar preference for the N-1-H protomer was assumed for the 8-iodo-9-methyladenine ion.

The ion-mobility-separated ions were further subjected to CID-MS$^2$, giving slightly different spectra for the isomers (Figure 2a–d). CID of both $\mathbf{BA1}^+$ and $\mathbf{BA2}^+$ resulted in the loss of bromine to produce adenine $C_5H_5N_5^{+\bullet}$ cation radicals at $m/z$ 135.0532 (Figure 2a,b). The major dissociation of both isomers was the loss of ammonia ($m/z$ 197) that was slightly more favored for $\mathbf{BA1}^+$. This difference in the loss of ammonia from 8-bromoadenine protomers was interesting in view of the complex mechanism for the loss of ammonia from protonated adenine that involves multiple skeletal isomerizations and proton migrations.[76,82] The formation of $C_5H_5N_5^{+\bullet}$ ($m/z$ 135.0535) by the loss of iodine was the dominant dissociation of $\mathbf{IA1}^+$ and $\mathbf{IA2}^+$ upon collisional activation (Figure 2c,d). This showed that $C_5H_5N_5^{+\bullet}$ cation radicals can be formed by the loss of the C-8 halogen atom upon CID to be further studied by MS$^n$ using UV–vis action spectroscopy and IMS.

The CID-MS$^2$ spectra of 8-bromo-9-methyladenine and 8-iodo-9-methyladenine ions (Figure S15a,b, Supporting Information) showed the loss of the halogen atoms, forming $C_6H_7N_5^{+\bullet}$ ions corresponding to methyladenine cation radicals. The loss of iodine was particularly facile, forming $C_6H_7N_5^{+\bullet}$ as the major fragment ion (Figure S15b).

**Cation Radicals.** The facile loss of bromine and iodine from the 8-substituted adenine and 9-methyladenine ions was utilized to generate the respective $C_5H_5N_5^{+\bullet}$ and $C_6H_7N_5^{+\bullet}$ ions that were further studied by UV–vis action spectroscopy and c-IMS. The canonical N-9-H isomer of the adenine cation radical ($\mathbf{A1}^{+\bullet}$)[48] and its N-3-H tautomer ($\mathbf{A2}^{+\bullet}$)[34] have been generated previously by reactions 1 and 3, respectively, as shown above in Scheme 1, and their UV–vis spectra have been reported. Those spectra are shown in Figure S16a,b (Supporting Information), so they could serve as a reference in the spectral assignment of dehalogenated adenine cation radicals. Briefly, the spectrum of ion $\mathbf{A1}^{+\bullet}$ is characterized by broad bands with maxima at 550 and 420 nm and UV bands at 330, 290, and 220 nm (Figure S16a). The spectrum of ion $\mathbf{A2}^{+\bullet}$ is distinguished by a broad band with a maximum at 520



https://doi.org/10.1021/acs.jpca.3c03179
J. Phys. Chem. A 2023, 127, 5899–5913

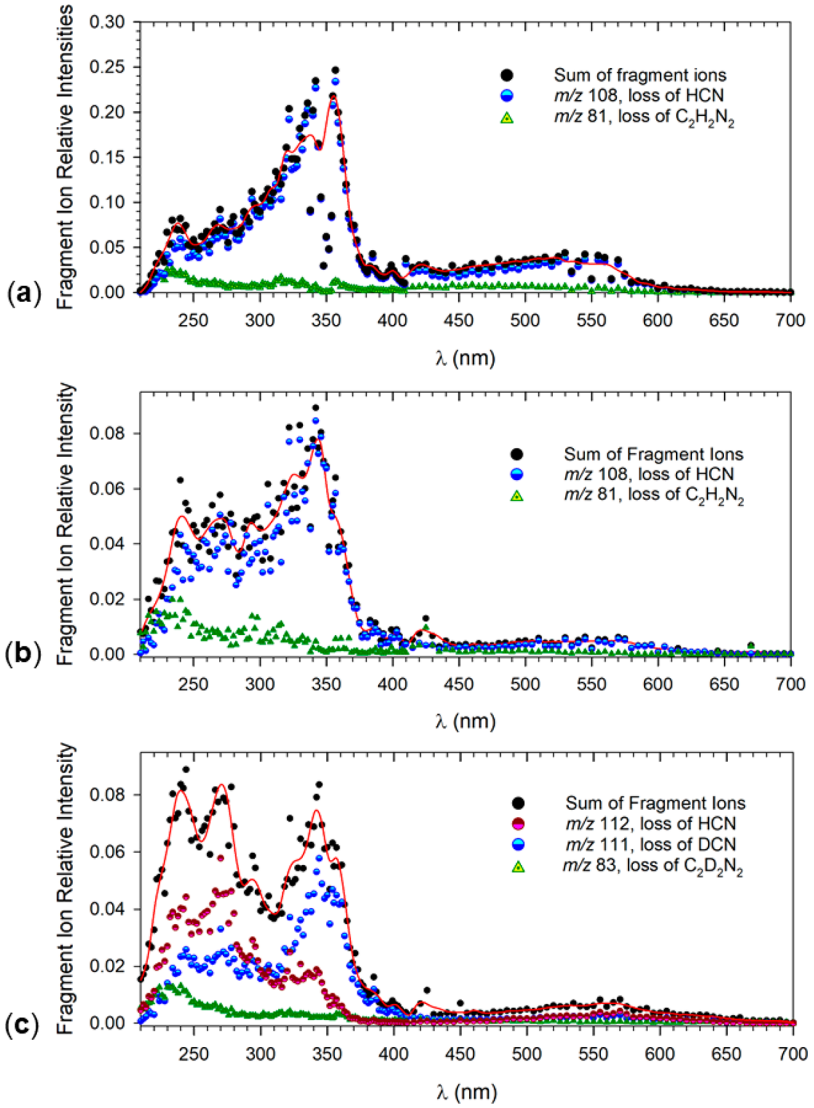


**Figure 3.** UV−vis action spectra of $C_5H_5N_5^{+\bullet}$ generated by CID-halogen loss from (a) 8-bromoadenine, (b) 8-iodoadenine, and (c) $C_5HD_4N_5^{+\bullet}$ from 8-iodo-[$D_4$]-adenine.

nm and a UV band at 340 nm that shows two shoulders at 305 and 260 nm as well as a separate weak band at 215 nm (Figure S16b). The UV−vis action spectrum of $C_5H_5N_5^{+\bullet}$ that was generated from $BA^+$ showed features that closely resembled those in the spectrum of **A2**$^{+\bullet}$ (Figure 3a). Namely, there was a broad band at 530 nm, a UV band with a maximum at 350 nm tailing to 250 nm, and a minor distinct band at 240 nm. The latter band intensity was enhanced by the contribution from the $m/z$ 81 photofragment channel (loss of $C_2H_2N_2$) that was stronger for the current $C_5H_5N_5^{+\bullet}$ isomer than for **A2**$^{+\bullet}$. In contrast, the UV−vis action spectrum of $C_5H_5N_5^{+\bullet}$ generated from $IA^+$ showed distinct features that were characterized by a diminished intensity of the band at 550 nm and the presence of additional UV bands at 240 and 270 nm that were carried by $m/z$ 108 (loss of HCN) and $m/z$ 81 (loss of $C_2H_2N_2$) channels (Figure 3b). This spectrum indicated the presence of additional $C_5H_5N_5^{+\bullet}$ isomers. These distinct features were amplified in the spectrum of the $C_5HD_4N_5^{+\bullet}$ derivative that was generated from $D_4$-$IA^+$ in which all exchangeable protons were replaced by deuterium. The spectrum of $C_5HD_4N_5^{+\bullet}$ showed major bands at 340, 270, and 240 nm (Figure 3c). It is worth noting that the wavelength profiles in the Figure 3c spectrum of the $m/z$ 112 (loss of HCN) and $m/z$ 111 (loss of DCN) photofragment ions differed, with the loss of DCN being favored at 350 nm, whereas the loss of HCN was prevalent at 270 and 240 nm. The loss of DCN at 350 nm was indicative of deuterium migration to C-8, forming $D_4$-**A2**$^{+\bullet}$; note that the loss of DCN has been reported as a major photodissociation channel of $D_3$-**A2**$^{+\bullet}$ at 340 nm (Figure S16c).[34]

To explore the $C_5H_5N_5^{+\bullet}$ ion structures, we obtained the CCSD(T)/CBS relative energies for several isomers (Table 1). These included various previously reported adenine tautomers (**A1**$^{+\bullet}$−**A7**$^{+\bullet}$),[34,48,83] C-8 radicals (**A8**$^{+\bullet}$−**A10**$^{+\bullet}$), and 8-aminopurine tautomers **A11**$^{+\bullet}$−**A14**$^{+\bullet}$ (Figure 4). The latter ions were included as putative products of skeletal rearrangement in **A8**$^{+\bullet}$−**A10**$^{+\bullet}$. The energy data showed that the C-8 radicals were relatively high-energy isomers of **A1**$^{+\bullet}$, having 0 K energies at 76, 79, and 132 kJ mol$^{-1}$ for **A8**$^{+\bullet}$, **A9**$^{+\bullet}$, and **A10**$^{+\bullet}$, respectively, relative to the most stable isomer **A1**$^{+\bullet}$. Ions **A8**$^{+\bullet}$−**A10**$^{+\bullet}$ were also less stable than the other $\pi$-radicals **A2**$^{+\bullet}$−**A7**$^{+\bullet}$, as well as 8-aminopurine isomers **A11**$^{+\bullet}$−**A14**$^{+\bullet}$, indicating the possibility of exergonic reactions of C-8 radicals by proton migration or skeletal rearrangements.



https://doi.org/10.1021/acs.jpca.3c03179
J. Phys. Chem. A 2023, 127, 5899−5913

**Table 1. Relative Energies and Collision Cross Sections of $C_5H_5N_5^{+\bullet}$ Isomers**

| | relative energy[a,b] | | |
|---|---|---|---|
| ion | M06-2X[c] | CCSD(T)/CBS[d] | CCS[e] |
| **A1**$^{+\bullet}$ | 0 | 0 | 129.0 |
| **A2**$^{+\bullet}$ | 24 | 21 | 128.7 |
| **A3**$^{+\bullet}$ | 21 | 21 | 129.6 |
| **A4**$^{+\bullet}$ | 43 | 46 | 129.4 |
| **A5**$^{+\bullet}$ | 66 | 58 | 131.8 |
| **A6**$^{+\bullet}$ | 53 | 46 | 132.6 |
| **A7**$^{+\bullet}$ | 56 | 65 | 132.8 |
| **A8**$^{+\bullet}$ | 77 | 76 | 127.3 |
| **A9**$^{+\bullet}$ | 80 | 79 | 126.6 |
| **A10**$^{+\bullet}$ | 133 | 132 | |
| **A11**$^{+\bullet}$ | 18 | 20 | 129.7 |
| **A12**$^{+\bullet}$ | 55 | 54 | 134.1 |
| **A13**$^{+\bullet}$ | 56 | 47 | 128.2 |
| **A14**$^{+\bullet}$ | 39 | 37 | |
| **A9**$^{+\bullet}$ → **TS1** | 207 | 208 | |
| **A9**$^{+\bullet}$ → **TS2** | 416 | 415 | |
| **A8**$^{+\bullet}$ → **TS3** | 253 | 257 | |

[a]In kJ mol$^{-1}$. [b]Including zero-point energies and referring to 0 K. [c]M06-2X/6-311++G(2d,p) optimized structures. [d]From single-point energies on M06-2X/6-311++G(2d,p) optimized structures. [e]Collision cross sections in $N_2$ (Å$^2$) calculated using the ion trajectory method with M06-2X/6-311++G(2d,p) optimized structures and Mulliken atom charge densities.

To aid the interpretation of the UV−vis action spectra and structure assignment of $C_5H_5N_5^{+\bullet}$ ions, we calculated vibronic spectra for **A3**$^{+\bullet}$**−A13**$^{+\bullet}$ to be compared with the experimental spectra. The spectra of **A3**$^{+\bullet}$**−A10**$^{+\bullet}$ are shown in Figure 5, and those of **A11**$^{+\bullet}$**−A14**$^{+\bullet}$ are given in Figure S17a−d (Supporting Information). The vibronic spectra of **A1**$^{+\bullet}$ and **A2**$^{+\bullet}$ have been reported previously[34,48] and are shown in Figure S17 (Supporting Information) for reference. The vibronic spectra of **A3**$^{+\bullet}$, **A4**$^{+\bullet}$, **A6**$^{+\bullet}$, and **A7**$^{+\bullet}$ showed bands in the visible region that were inconsistent with the action spectra in Figure 3b,c. The presence of the bands at 240 and 270 nm in the Figure 3b,c action spectra can be accounted for by isomers **A8**$^{+\bullet}$**−A10**$^{+\bullet}$. Out of these, C-8 radicals **A8**$^{+\bullet}$ and **A9**$^{+\bullet}$ had protonation patterns that were directly related to the precursor IA$^+$ ions. Structure **A10**$^{+\bullet}$ was the highest-energy isomer whose formation would require endergonic proton migrations to N-9 and N-7 which was deemed less probable. The vibronic spectra of the 8-aminopurine isomers showed some common features with action spectra (Figure S17). This was particularly visible for the spectra of **A11**$^{+\bullet}$ and **A12**$^{+\bullet}$ (Figure S17a,b, respectively) that showed strong bands at 270 and 250 nm, respectively, which coincided with analogous bands in the Figure 5b,c spectra. The broad bands at 350 nm in the vibronic spectra of **A11**$^{+\bullet}$ and **A12**$^{+\bullet}$ could be present in the Figure 5b,c action spectra, where they would be overlapped by the strong band of **A2**$^{+\bullet}$. The vibronic spectra of **A13**$^{+\bullet}$ and **A14**$^{+\bullet}$ were less compatible with the action spectra as both were showing bands in the visible region.

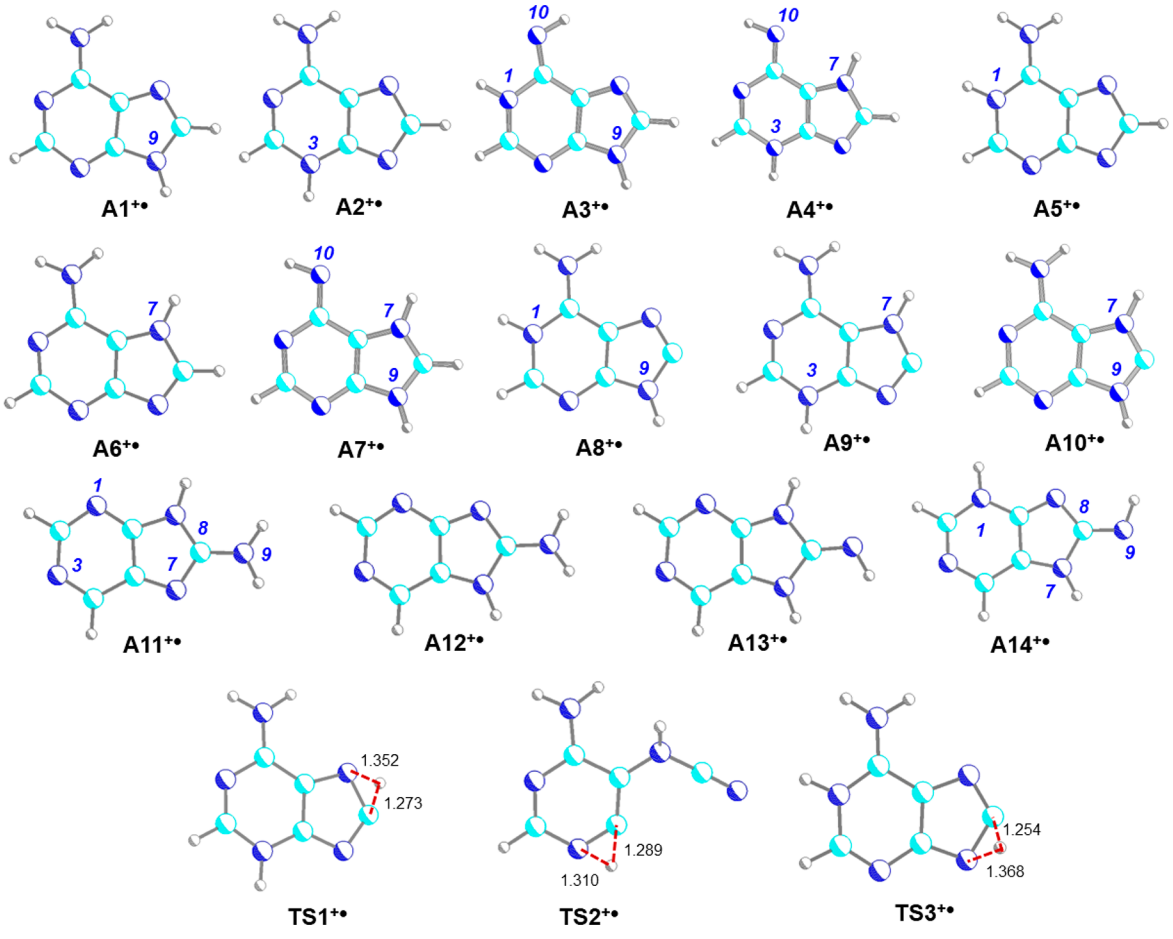


**Figure 4.** M06-2X/6-311++G(2d,p) optimized structures of adenine-related $C_5H_5N_5^{+\bullet}$ isomers.



https://doi.org/10.1021/acs.jpca.3c03179
J. Phys. Chem. A 2023, 127, 5899−5913

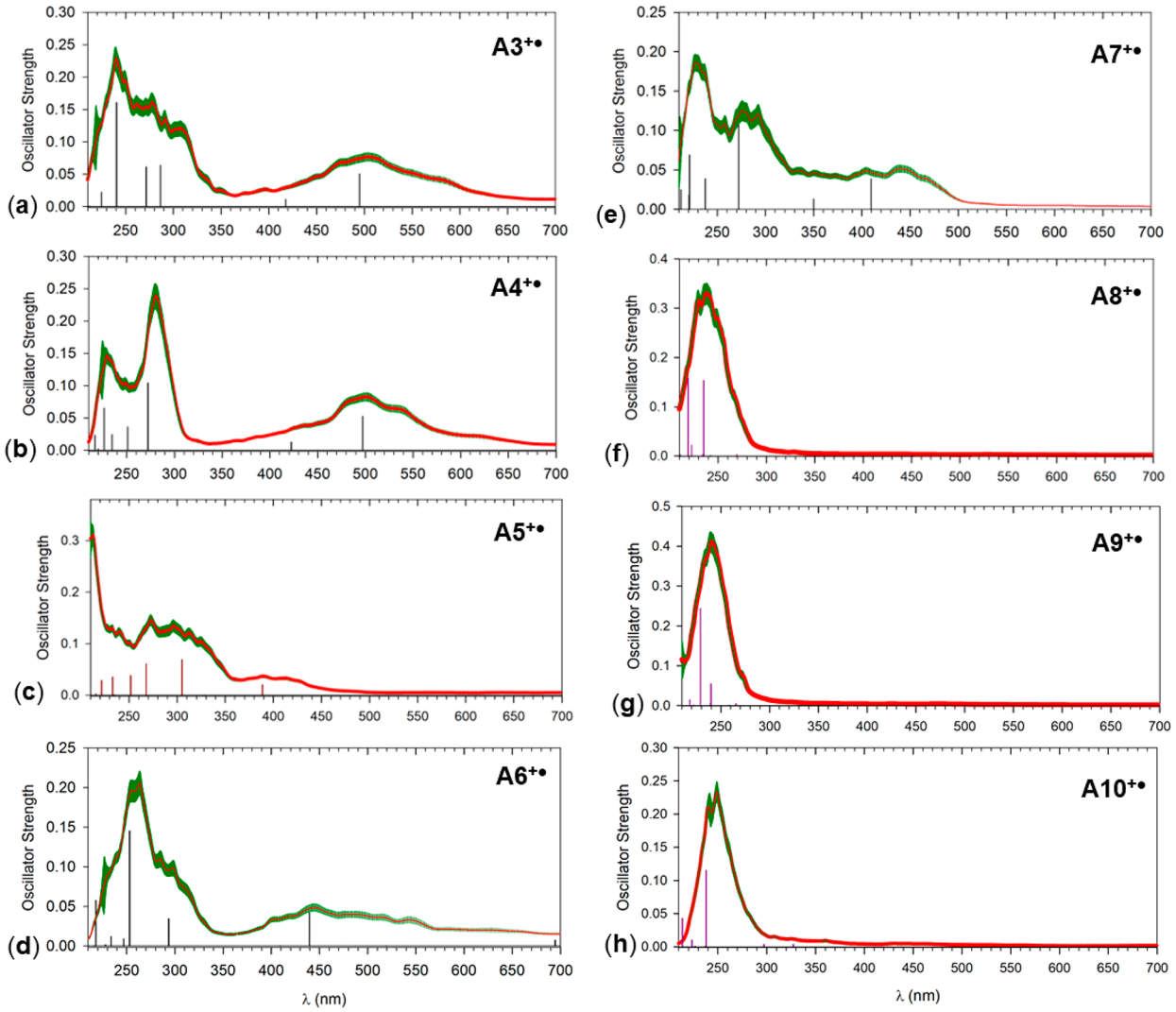


**Figure 5.** M06-2X/6-31+G(d,p) calculated vibronic absorption spectra of $A3^{+\bullet}$–$A10^{+\bullet}$ from 300 configurations at 350 K.

The presence of spectroscopically compatible isomers $A11^{+\bullet}$ and $A12^{+\bullet}$ was considered *vis-a-vis* their formation from $A8^{+\bullet}$ and $A9^{+\bullet}$. In both cases, the isomerization would involve ring cleavage, multiple proton transfers, and ring closure, as shown in Scheme 3.

Ion $A9^{+\bullet}$ was considered to undergo competitive 1,2-migration of N-7-H (path *a*) that proceeded via **TS1** at 208 kJ $mol^{-1}$, forming isomer $A2^{+\bullet}$ at −58 kJ $mol^{-1}$, both relative to $A9^{+\bullet}$. Because of its exergonicity, this isomerization was kinetically irreversible. The alternative ring-opening pathway (*b*, Scheme 3) involved intermediate $A15^{+\bullet}$ that was at 92 kJ $mol^{-1}$ relative to $A9^{+\bullet}$. Further isomerization by 1,2-hydrogen atom migration from N-3 to C-4 was calculated to proceed via a high-energy transition state (**TS2**, 415 kJ $mol^{-1}$ relative to $A9^{+\bullet}$) to form the nitrile isomer $A16^{+\bullet}$ that was at 156 kJ $mol^{-1}$ relative to $A9^{+\bullet}$. Both the high energy of **TS2** and the continuously endergonic character of this reaction sequence should make it incompatible with path *a*, despite the overall exergonic isomerization to $A13^{+\bullet}$ and $A11^{+\bullet}$. On the basis of this analysis, we concluded that the formation of the 8-aminopurine tautomers should be excluded. Path *a* and the related proton migration to C-8 were analogous to the isomerization of $A8^{+\bullet}$ to $A5^{+\bullet}$ that was 10 kJ $mol^{-1}$ exergonic and proceeded via **TS3** at 257 kJ $mol^{-1}$ relative to $A8^{+\bullet}$ (Table 1).

Both isomerizations were expected to show primary and higher-order isotope effects on the migration of deuterium in $C_5HD_4N_5^{+\bullet}$. We used RRKM calculations to obtain unimolecular rate constants in order to assess the isotope effects in the energy intervals that would result in 10−90% isomerization on the experimental time scale of 10−50 ms (Figure S18a,b, Supporting Information). The Figure S18a data shows that $A8^{+\bullet}$ underwent 90% isomerization by N-9-H → C-8 hydrogen migration after 10 ms at an internal energy of 352 kJ $mol^{-1}$. At the same internal energy, $D_4$-$A8^{+\bullet}$ was isomerized by deuterium migration by only 38%. Similarly, 90% hydrogen migration in $A8^{+\bullet}$ after 50 ms was achieved at an internal energy of 333 kJ $mol^{-1}$, whereby $D_4$-$A8^{+\bullet}$ underwent only 32% deuterium migration at the same internal energy. Very similar results were obtained from RRKM calculations of rate constants for N-7-H → C-8 hydrogen and deuterium migration in $A9^{+\bullet}$ and $D_4$-$A9^{+\bullet}$ where the lower **TS1** energy allowed isomerization to occur at lower internal energies (Figure S18b) compared to those in $A8^{+\bullet}$. The calculated isotope effects were consistent with the UV−vis action spectra of $C_5H_5N_5^{+\bullet}$ ions shown in Figure 3b,c; the bands at 240 and 270 nm that were assignable to $A8^{+\bullet}$ or $A9^{+\bullet}$ were substantially


https://doi.org/10.1021/acs.jpca.3c03179
J. Phys. Chem. A 2023, 127, 5899−5913

Scheme 3. Isomerization Pathways of $A9^{+\bullet}$[a]

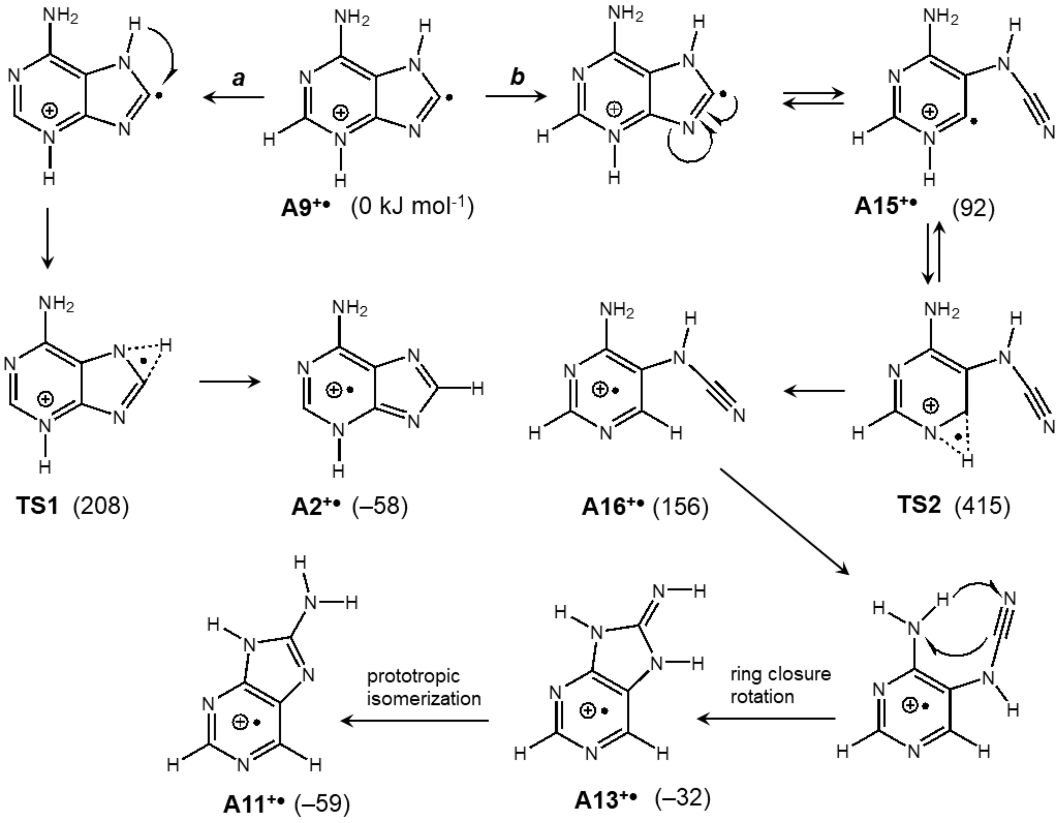


[a]Relative energies are from single-point CCSD(T)/CBS calculations on M06-2X/6-311++G(2d,p) optimized geometries, include zero-point vibrational energies, and refer to 0 K.

enhanced upon deuteration due to their slower isomerization to $A5^{+\bullet}$ or $A2^{+\bullet}$, respectively.

**9-Methyladenine Cation Radicals.** The techniques described above for the generation and study of adenine cation radicals were also implemented for $C_6H_7N_5^{+\bullet}$ ions from 8-bromo-9-methyladenine (BMA) and 8-iodo-9-methyladenine (IMA). The action spectrum of $C_6H_7N_5^{+\bullet}$ from BMA (Figure 6a) showed a broad band at 560 nm and a composite band with a maximum at 340 nm and shoulders at 300, 270, and 220 nm. The main photofragment channels contributing to these bands were the loss of H ($m/z$ 148) and the loss of hydrogen cyanide ($m/z$ 122). The action spectrum of the H/D exchanged ion, $C_6H_4D_3N_5^{+\bullet}$, displayed very similar features, with slightly enhanced peaks appearing at 270 and 220 nm (Figure 6b). These additional features were even more amplified in the action spectrum of $C_6H_7N_5^{+\bullet}$ from IMA that showed bands with distinct maxima at 270 and 220 nm and less distinct bands at 360 and 310 nm (Figure 6c). To interpret the spectra and assign structures to the $C_6H_7N_5^{+\bullet}$ ions, we calculated the optimized structures, relative energies, and vibronic spectra of several isomers. Previous studies have identified the canonical 9-methyladenine cation radical (**MA1**$^{+\bullet}$) and its N-1-H-9-methylene distonic isomer (**MA2**$^{+\bullet}$) as the lowest-energy ions that have been characterized by their action spectra. These are shown in Figure S19a,b (Supporting Information) as a reference. The optimized structures of several $C_6H_7N_5^{+\bullet}$ isomers and their relative energies are shown in Figure 7. The data show that the C-8 radicals **MA6**$^{+\bullet}$–**MA8**$^{+\bullet}$ that differed in the protonation site were high-energy isomers of both canonical ion **MA1**$^{+\bullet}$ and lowest-energy distonic isomer **MA2**$^{+\bullet}$. Among the C-8-radicals, N-1-H tautomer **MA6**$^{+\bullet}$ had the lowest energy at 92 kJ mol$^{-1}$ relative to **MA2**$^{+\bullet}$. The highly exergonic isomerization of **MA6**$^{+\bullet}$ by a hydrogen migration from the 9-methyl to C-8, forming **MA2**$^{+\bullet}$, was calculated to require 203 kJ mol$^{-1}$ in the transition state (**TS4**). However, the UV–vis action spectrum of **MA2**$^{+\bullet}$ (Figure S19b) was distinctly different from the spectrum of the $C_6H_7N_5^{+\bullet}$ ion from IMA. In particular, the Figure 6c spectrum lacked the distinct band at 400 nm that was characteristic of **MA2**$^{+\bullet}$.[81] Another exergonic isomerization by methyl group migration to C-8, forming the C-8-methyl isomer **MA9**$^{+\bullet}$, required 273 kJ mol$^{-1}$ in **TS5**. However, the calculated vibronic spectrum of **MA9**$^{+\bullet}$ (Figure 8d) was incompatible with the distinct features in the UV–vis action spectrum; notably, it lacked the prominent band at 270 nm shown in Figure 6c. We found several cation radical isomers that had calculated vibronic spectra that were compatible with the experimental 270 nm band. Those were the C-8 radical protomers **MA6**$^{+\bullet}$, **MA7**$^{+\bullet}$, and **MA8**$^{+\bullet}$ that showed prominent absorption bands at 250 nm but very weak absorption above 400 nm (Figure 8a–c). Two isomers with rearranged skeletons, **MA10**$^{+\bullet}$ and **MA11**$^{+\bullet}$, were also calculated to have absorption bands at 270 nm. We note that these would have resulted from a ring opening and a skeletal rearrangement in **MA2**$^{+\bullet}$. However, the energy data (Table 2) indicate that these rearrangements would have been 71–81 kJ mol$^{-1}$ endergonic and therefore disfavored.

In view of the absence of **MA2**$^{+\bullet}$ among the $C_6H_7N_5^{+\bullet}$ ions, the formation of **MA10**$^{+\bullet}$ and **MA11**$^{+\bullet}$ can be excluded. The spectroscopic evidence indicated that the band at 270 nm in


https://doi.org/10.1021/acs.jpca.3c03179
J. Phys. Chem. A 2023, 127, 5899–5913

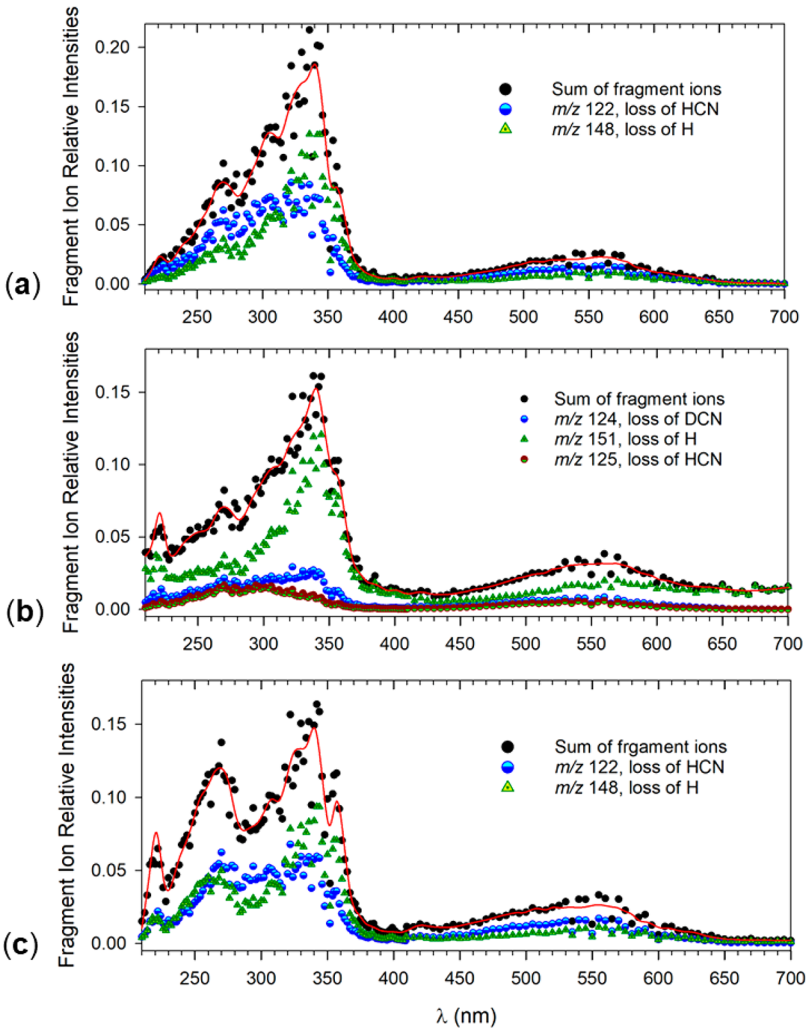


**Figure 6.** UV−vis action spectra of $C_6H_7N_5^{+\bullet}$ ions generated by CID-halogen loss from (a) 9-methyl-8-bromoadenine, (b) $C_6H_4D_3N_5^{+\bullet}$ from 9-methyl-8-bromo-[$D_3$]-adenine, and (c) 9-methyl-8-iodoadenine.

the spectrum of $C_6H_7N_5^{+\bullet}$ could be assigned to a C-8 radical; of those, the N-1-H protomer **MA6**$^{+\bullet}$ had the lowest energy, and its protonation site correlated with that of the most stable IMA precursor ion. However, the spectrum of **MA6**$^{+\bullet}$ alone was insufficient to explain the other bands in the action spectrum. The presence of the broad band at 550 nm and the composite band at 340 nm strongly indicated the presence of the canonical isomer **MA1**$^{+\bullet}$ (cf. the reference action spectrum in Figure S19a). It is not clear how **MA1**$^{+\bullet}$ was produced upon CID of the IMA ion because a unimolecular hydrogen migration from N-1 to C-8 would have faced several high-energy steps. We posit that the isomerization was catalyzed by the departing halogen atom forming a transient $[C_6H_6N_5 . . .HX]^+$ complex that can deliver the hydrogen atom to C-8. Our calculated dissociation energy of the C-8−Br bond in the BMA ion (354 kJ mol$^{-1}$ by M06-2X/aug-cc-pVTZ) was similar to that reported for neutral 8-bromoadenine.[42] This was less than the dissociation energy needed for HBr elimination from the BMA ion, giving singlet or triplet $C_6H_6N_5^+$ ions at their respective thermochemical thresholds of 480 and 405 kJ mol$^{-1}$ (Scheme S4, Supporting Information). This indicated that a $[C_6H_6N_5 . . .HBr]^+$ complex would favor a hydrogen transfer followed by the loss of the Br atom.

**Ion Mobility of Cation Radicals.** To further characterize the $C_5H_5N_5^{+\bullet}$ ions, we carried out cyclic ion mobility measurements of ions generated by CID of protonated 8-bromo and 8-iodoadenine, **BA**$^+$ and **IA**$^+$, respectively. The cation radical intensities showed a 50- to 100-fold decrease after several cycles in the c-IMS, although the residual ion intensities were sufficient for arrival time evaluation. The c-IMS profiles obtained after three cycle passes showed multiple peaks for $C_5H_5N_5^{+\bullet}$ (Figure 9). Upon applying Gaussian fitting to the arrival time profiles, we distinguished three main components at 39.6, 41.1, and 43.4 ms along with two minor components at 40.2 and 42.5 ms. The major components were assigned to CCS = 130.4 (±0.7), 132.5 (±0.5), and 134.7 (±0.7) Å$^2$ for the ions generated from **BA**$^+$ (Figure 9a) and to CCS = 130.2 (±0.7), 131.8 (±0.5), and 134.6 (±0.7) Å$^2$ for the ions generated from **IA**$^+$ after peak extraction by Gaussian fitting (Figure 9b). Considering the reproducibility of these measurements, the CCS for the well-resolved peaks was presumed to be identical to those of the $C_5H_5N_5^{+\bullet}$ ions from **BA**$^+$ and **IA**$^+$. The relative intensities of the major peaks differed for $C_5H_5N_5^{+\bullet}$ ions generated from **BA**$^+$ and **IA**$^+$, as the former showed a major component with CCS = 130.4 Å$^2$ while the latter had a larger component at CCS = 134.5 Å$^2$. However, the very substantial decrease in the IMS-separated


https://doi.org/10.1021/acs.jpca.3c03179
J. Phys. Chem. A 2023, 127, 5899−5913

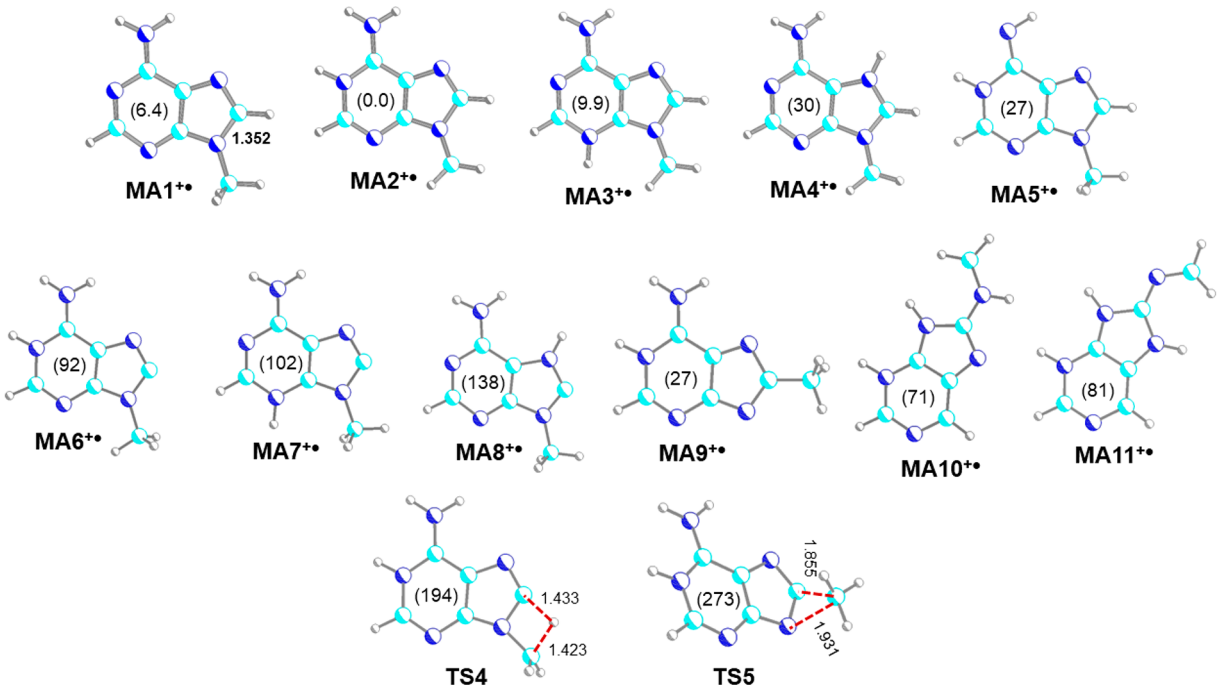


**Figure 7.** M06-2X/6-311++G(2d,p) optimized structures and CCSD(T)/CBS relative energies of selected $C_6H_7N_5^{+\bullet}$ isomers at 0 K.

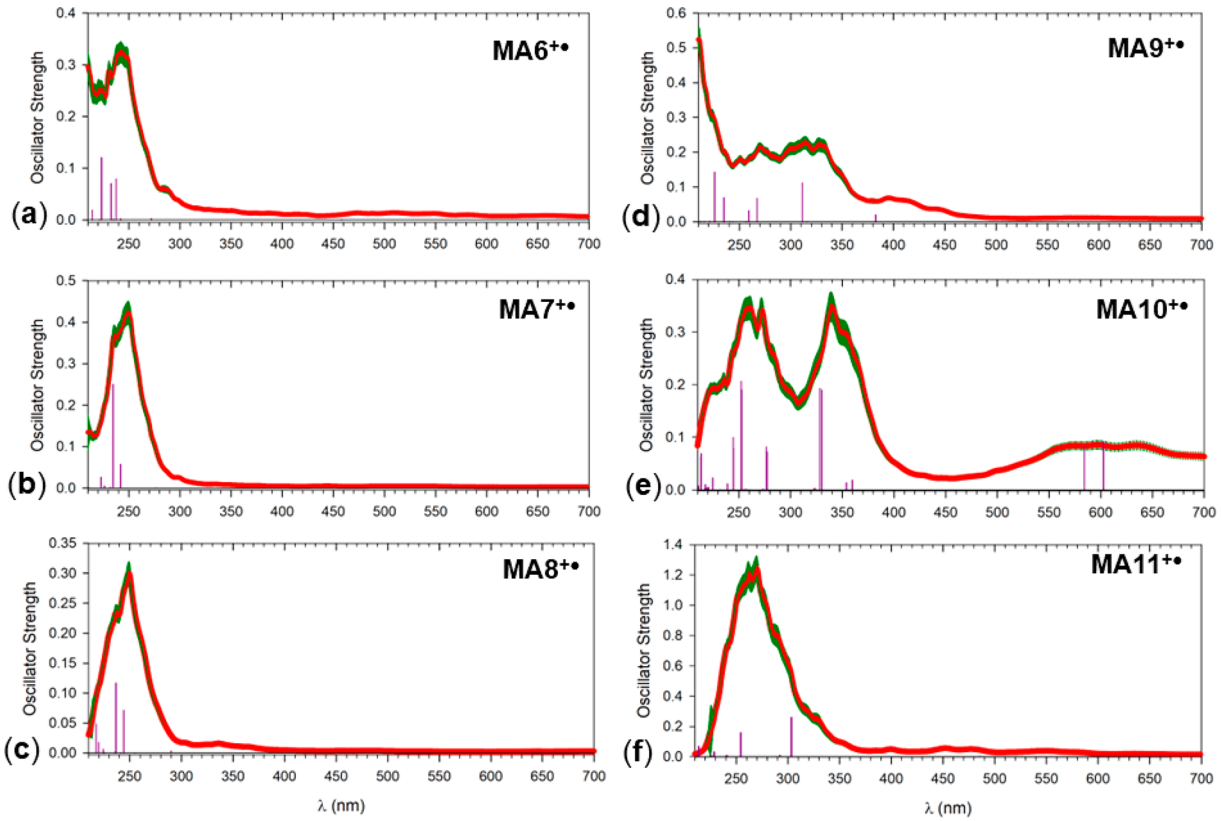


**Figure 8.** M06-2X/6-31+G(d,p) calculated vibronic spectra of **MA6**$^{+\bullet}$**−MA11**$^{+\bullet}$ from 300 configurations at 350 K.

ion intensities could affect the ions differently and skew their relative intensities.

To assign these major components, we utilized $C_5H_5N_5^{+\bullet}$ internal standards that were generated by the CID of [Cu(terpy) adenine]$^{2+\bullet}$ complexes. These were shown previously by UV−vis action spectroscopy to chiefly consist of the canonical **A1**$^{+\bullet}$ isomer and accordingly provided a single major peak in c-IMS (Figure S20, Supporting Information) that had CCS = 132 (±0.8) Å$^2$. Since the doubly charged [Cu(terpy) adenine]$^{2+\bullet}$ complex and **BA**$^+$ had similar $m/z$ values of 215.5 and 214, respectively, we were able to isolate them simultaneously for CID and co-generate the respective



https://doi.org/10.1021/acs.jpca.3c03179
J. Phys. Chem. A 2023, 127, 5899−5913

Table 2. Relative Energies of $C_6H_7N_5^{+\bullet}$ Isomers

| | relative energy[a,b] | |
|---|---|---|
| ion | M06-2X[c] | CCSD(T)/CBS[d] |
| **MA1**$^{+\bullet}$ | 6.0 | 6.4 |
| **MA2**$^{+\bullet}$ | 0 | 0 |
| **MA3**$^{+\bullet}$ | 10 | 9.9 |
| **MA4**$^{+\bullet}$ | 30 | 30 |
| **MA5**$^{+\bullet}$ | 29 | 27 |
| **MA6**$^{+\bullet}$ | 87 | 92 |
| **MA7**$^{+\bullet}$ | 96 | 102 |
| **MA8**$^{+\bullet}$ | 134 | 137 |
| **MA9**$^{+\bullet}$ | 25 | 27 |
| **MA10**$^{+\bullet}$ | 66 | 71 |
| **MA11**$^{+\bullet}$ | 72 | 81 |
| **MA6**$^{+\bullet}$ → **TS4** | 203 | 194 |
| **MA6**$^{+\bullet}$ → **TS5** | 274 | 273 |

[a]In kJ mol$^{-1}$. [b]Including zero-point energies and referring to 0 K. [c]M06-2X/6-311++G(2d,p) optimized structures. [d]From single-point energies on M06-2X/6-311++G(2d,p) optimized structures.

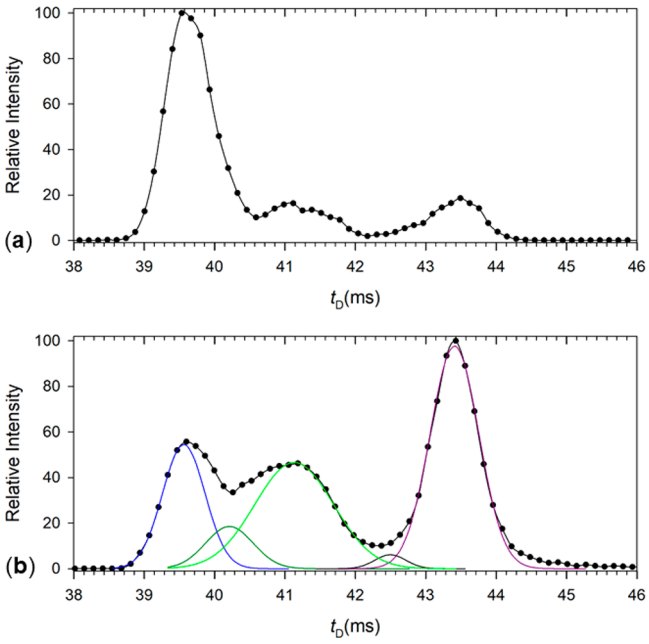


**Figure 9.** Arrival time profiles after three cycle passes in c-IMS of $C_5H_5N_5^{+\bullet}$ ions from (a) 8-bromoadenine and (b) 8-iodoadenine.

$C_5H_5N_5^{+\bullet}$ ions for c-IMS. Similarly, by tuning the $m/z$ of the Cu complex with a 4′-*p*-fluorophenyl-2,2′;6′,2″-terpyridine ligand we shifted the $m/z$ of the doubly charged precursor ion to 262.5 so that it could be co-isolated for CID with **IA**$^+$ ($m/z$ 262) and used to co-generate **A1**$^{+\bullet}$ along with $C_5H_5N_5^{+\bullet}$ ions from **IA**$^+$. The UV−vis action spectrum of $C_5H_5N_5^{+\bullet}$ from the [Cu(4′-*p*-fluorophenyl-2,2′;6′,2″-terpyridine) adenine]$^{2+\bullet}$ complex was checked and found to be identical to that of **A1**$^{+\bullet}$ (Figure S16a).[48] The isobaric $C_5H_5N_5^{+\bullet}$ ions from these different precursors were readily distinguished by plotting their intensities as a function of collision energy. At the same ion acceleration voltage, the doubly charged complexes gained twice as much kinetic energy and thus underwent CID at lower voltage settings. This is illustrated by arrival time profiles in Figure 10 where the peak of **A1**$^{+\bullet}$ at $t_D$ = 41.1 ms from the Cu complex appeared at the lowest energy and its relative intensity then gradually decreased at higher collision energies, while

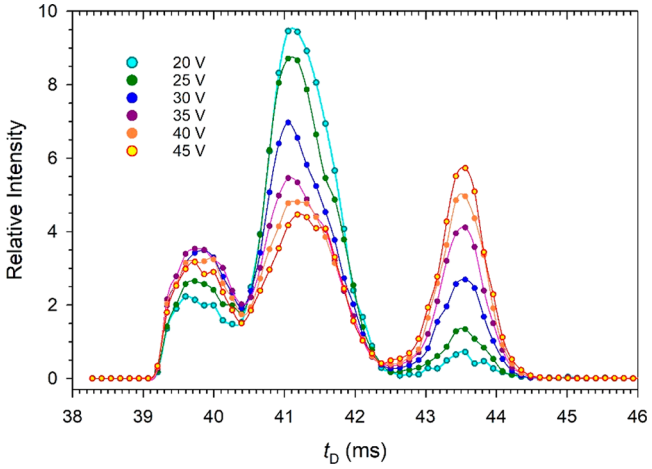


**Figure 10.** Energy-dependent arrival time profiles of $C_5H_5N_5^{+\bullet}$ ions cogenerated from the [Cu(4′-*p*-fluorophenyl-2,2′;6′,2″-terpyridine) adenine]$^{2+\bullet}$ complex and **IA**$^+$.

those of the peaks at $t_D$ = 39.8 and 43.5 ms increased. Note that the integrated band intensities in Figure 10 are plotted relative to the total $C_5H_5N_5^{+\bullet}$ ion count at each energy, so a decrease in one band intensity is related to an increase in the others. We note that the shape and width of the peaks at 39.8 and 41.1 ms indicated the presence of unresolved minor components, which were also apparent in the profile shown in Figure 9b. Interestingly, the relative intensities of these bands also changed as a function of collision energy, with the band at $t_D$ = 43.5 ms gaining prominence at 45 V. The composite arrival time profiles in Figure 10 allowed us to compare the theoretical CCS of $C_5H_5N_5^{+\bullet}$ isomers using the CCS of **A1**$^{+\bullet}$ as a reference. The calculated CCS showed values within the range of 126.6−134.1 Å$^2$ (Table 1). Some of the isomers had barely distinguishable theoretical CCS, such as for **A3**$^{+\bullet}$, **A4**$^{+\bullet}$, and **A11**$^{+\bullet}$ and **A6**$^{+\bullet}$ and **A7**$^{+\bullet}$. Therefore, we utilized the information gleaned from the UV−vis action spectra and combined it with the c-IMS and calculated CCS data. According to Figure 10, the $C_5H_5N_5^{+\bullet}$ isomers produced from **BA**$^+$ and **IA**$^+$ had arrival times that coincided with that of **A1**$^{+\bullet}$ or flanked it according to their smaller or larger CCS. This pointed to **A5**$^{+\bullet}$ and **A6**$^{+\bullet}$ for ions with CCS larger than that of **A1**$^{+\bullet}$ representing the last peak in the arrival time profile. Ions **A8**$^{+\bullet}$ and **A9**$^{+\bullet}$ that had a CCS smaller than that of **A1**$^{+\bullet}$ could be assigned to the first peak in the Figure 9 arrival time profiles. The peak in the middle could be assigned to **A2**$^{+\bullet}$ whose formation was strongly indicated by the UV−vis action spectrum. We did not attempt to interpret the different relative intensities of the $C_5H_5N_5^{+\bullet}$ ion arrival time peaks and their relationship to the band intensities in the action spectra. Regarding the c-IMS data, the $C_5H_5N_5^{+\bullet}$ ion intensities underwent a very substantial loss by being driven in multiple cycles through the traveling wave device, so discrimination could not be excluded. The value of the c-IMS measurements was that they confirmed that multiple $C_5H_5N_5^{+\bullet}$ isomers were formed by CID and allowed us to roughly distinguish them relative to the **A1**$^{+\bullet}$ internal standard.

## CONCLUSIONS

The formation of adenine and 9-methyladenine cation radicals with a $\sigma$-radical defect at C-8 was found to be accompanied by rearrangements, forming more stable $\pi$-radicals. The rearrange-


https://doi.org/10.1021/acs.jpca.3c03179
J. Phys. Chem. A 2023, 127, 5899−5913

ments were driven by the thermodynamic instability of the σ-radicals, which all represented high-energy species. Moderating the energetics of the cation radical formation, such as by using the dissociation of the weak C-8−I bond and slowing the isomerization by implementing deuterium isotope effects, resulted in an increased yield of adenine C-8 σ-radicals. An analysis of the adenine cation radicals by multipass cyclic ion mobility mass spectrometry allowed us to distinguish isomers and assess their CCS that were compared with theoretical values. By using a combination of UV−vis action spectroscopy and c-IMS data, we were able to identify adenine C-8 σ-radicals and their major isomerization products. The combination of these techniques represents a powerful tool for the structure elucidation of transient ion species, including elusive high-energy isomers in the gas phase.

## ■ ASSOCIATED CONTENT

### Supporting Information

The Supporting Information is available free of charge at https://pubs.acs.org/doi/10.1021/acs.jpca.3c03179.

Description of synthetic procedures with compound spectroscopic characterization, additional figures including NMR and mass spectra, and reaction schemes and energies from DFT calculations (PDF)

## ■ AUTHOR INFORMATION


### Corresponding Author

**František Tureček** − *Department of Chemistry, University of Washington, Washington 98195-1700, United States;* orcid.org/0000-0001-7321-7858; Phone: +1-206-685-2041; Email: turecek@uw.edu

### Authors

**Václav Zima** − *Department of Chemistry, University of Washington, Washington 98195-1700, United States*

**Mikuláš Vlk** − *Institute of Organic Chemistry and Biochemistry, Czech Academy of Sciences, 16610 Prague 6, Czech Republic; Department of Analytical Chemistry, Faculty of Science, Charles University, 12800 Prague, Czech Republic*

**Jiahao Wan** − *Department of Chemistry, University of Washington, Washington 98195-1700, United States*

**Josef Cvačka** − *Institute of Organic Chemistry and Biochemistry, Czech Academy of Sciences, 16610 Prague 6, Czech Republic; Department of Analytical Chemistry, Faculty of Science, Charles University, 12800 Prague, Czech Republic*

Complete contact information is available at: https://pubs.acs.org/10.1021/acs.jpca.3c03179


### Author Contributions

‖V.Z. and M.V. contributed equally to this work, and both should be considered first authors.

### Notes

The authors declare no competing financial interest.

## ■ ACKNOWLEDGMENTS

Support by the Chemistry Division of the U.S. National Science Foundation (grant CHE-1951518) and the Klaus and Mary Ann Saegebarth Endowment is gratefully acknowledged. Thanks are due to Dr. Yue Liu for adapting the ion trajectory parameters for Br and I from refs 72 and 73 into the Mobcal Fortran code. M.V. and J.C. acknowledge partial support by Charles University project SVV260690.

## ■ REFERENCES


(1) Cadet, J.; Douki, T.; Ravanat, J.-L. Oxidatively Generated Damage to the Guanine Moiety of DNA: Mechanistic Aspects and Formation in Cells. *Acc. Chem. Res.* **2008**, *41*, 1075−1083.

(2) Jones, A. S.; Woodhouse, D. L. Bromination of Nucleic Acids and Their Derivatives. *Nature* **1959**, *183*, 1603−1605.

(3) Duval, J.; Ebel, J. P. Chlorination of Yeast Soluble RNA in a Dimethylformamide Medium. *C. R. Acad. Hebd. Seances Acad. Sci. D* **1966**, *263*, 1773−1776.

(4) Ikehara, M.; Uesugi, S.; Kaneko, M. Bromination of Adenine Nucleoside and Nucleotide. *Chem. Commun.* **1967**, 17−18.

(5) Rayala, R.; Wnuk, S. F. Bromination at C-5 of Pyrimidine and C-8 of Purine Nucleosides with 1,3-Dibromo-5,5-Dimethylhydantoin. *Tetrahedron Lett.* **2012**, *53*, 3333−3336.

(6) Blasiak, L. C.; Drennan, C. L. Structural Perspective on Enzymatic Halogenation. *Acc. Chem. Res.* **2009**, *42*, 147−155.

(7) van Pee, K.-H. Enzymatic Chlorination and Bromination. *Enzymatic Chlorination and Bromination*; Methods in Enzymology; Elsevier, 2012; Vol. *516*, pp 237−257.

(8) Agarwal, V.; Miles, Z. D.; Winter, J. M.; Eustaquio, A. S.; El Gamal, A. A.; Moore, B. S. Enzymatic Halogenation and Dehalogenation Reactions: Pervasive and Mechanistically Diverse. *Chem. Rev.* **2017**, *117*, 5619−5674.

(9) Liu, N.; Ban, F.; Boyd, R. J. Modeling Competitive Reaction Mechanisms of Peroxynitrite Oxidation of Guanine. *J. Phys. Chem. A* **2006**, *110*, 9908−9914.

(10) Kumar, A.; Sevilla, M. D. π- vs σ-Radical States of One-Electron-Oxidized DNA/RNA Bases: A Density Functional Theory Study. *J. Phys. Chem. B* **2013**, *117*, 11623−11632.

(11) Rokhlenko, Y.; Cadet, J.; Geacintov, N. E.; Shafirovich, V. Mechanistic Aspects of Hydration of Guanine Radical Cations in DNA. *J. Am. Chem. Soc.* **2014**, *136*, 5956−5962.

(12) Sun, Y.; Tsai, M.; Moe, M. M.; Liu, J. Dynamics and Multiconfiguration Potential Energy Surface for the Singlet O2 Reactions with Radical Cations of Guanine, 9-Methylguanine, 2′-Deoxyguanosine, and Guanosine. *J. Phys. Chem. A* **2021**, *125*, 1564−1576.

(13) Sun, Y.; Zhou, W.; Moe, M. M.; Liu, J. Reactions of Water with Radical Cations of Guanine, 9-Methylguanine, 2'-Deoxyguanosine and Guanosine: Keto-Enol Isomerization, C8-hydroxylation, and Effects of N9-substitution. *Phys. Chem. Chem. Phys.* **2018**, *20*, 27510−27522.

(14) Uvaydov, Y.; Geacintov, N. A.; Shafirovich, V. Generation of Guanine-Amino Acid Cross-Links by a Free Radical Combination Mechanism. *Phys. Chem. Chem. Phys.* **2014**, *16*, 11729−11736.

(15) Zhou, W.; Liu, J. Reaction Mechanism and Dynamics for C8-hydroxylation of 9-Methylguanine Radical Cation by Water Molecules. *Phys. Chem. Chem. Phys.* **2021**, *23*, 24464−24477.

(16) Steenken, S. Purine Bases, Nucleosides, and Nucleotides: Aqueous Solution Redox Chemistry and Transformation Reactions of \ Their Radical Cations and e- and OH Adducts. *Chem. Rev.* **1989**, *89*, 503−520.

(17) Candeias, L. P.; Steenken, S. Electron Adducts of Adenine Nucleosides and Nucleotides in Aqueous Solution: Protonation at Two Carbon Sites (C2 and C8) and Intra- and Intermolecular Catalysis by Phosphate. *J. Phys. Chem. A* **1992**, *96*, 937−944.

(18) Candeias, L. P.; Wolf, P.; O'Neill, P.; Steenken, S. Reaction of Hydrated Electrons with Guanine Nucleosides: Fast Protonation on Carbon of the Electron Adduct. *J. Phys. Chem. A* **1992**, *96*, 10302−10307.

(19) Barnes, J.; Bernhard, W. A. The Protonation State of One-Electron Reduced Cytosine and Adenine. 1. Initial Protonation Sites at Low Temperatures in Glassy Solids. *J. Phys. Chem. A* **1993**, *97*, 3401−3408.

(20) Barnes, J.; Bernhard, W. A. One-Electron-Reduced Cytosine in Acidic Glasses: Conformational States before and after Proton Transfer. *J. Phys. Chem. A* **1994**, *98*, 10969−10977.

(21) Steenken, S.; Jovanovic, S. V. How Easily Oxidizable Is DNA? One- Electron Reduction Potentials of Adenosine and Guanosine Radicals in Aqueous Solution. *J. Am. Chem. Soc.* **1997**, *119*, 617−618.
(22) Gatlin, C. L.; Tureček, F.; Vaisar, T. Copper(II) Amino Acid Complexes in the Gas Phase. *J. Am. Chem. Soc.* **1995**, *117*, 3637−3638.
(23) Turećek, F. Copper-Biomolecule Complexes in the Gas Phase. The Ternary Way. *Mass Spectrom. Rev.* **2007**, *26*, 563−582.
(24) Wee, S.; O'Hair, R. A. J.; McFadyen, W. D. Can Radical Cations of the Constituents of Nucleic Acids Be Formed in the Gas Phase Using Ternary Transition Metal Complexes? *Rapid Commun. Mass Spectrom.* **2005**, *19*, 1797−1805.
(25) Lam, A. K.; Abrahams, B. F.; Grannas, M. J.; McFadyen, W. D.; O'Hair, R. A. J. Tuning the Gas Phase Redox Properties of Copper(II) Ternary Complexes of Terpyridines to Control the Formation of Nucleobase Radical Cations. *Dalton Trans.* **2006**, 5051−5061.
(26) Hoshika, S.; Leal, N. A.; Kim, M.-J.; Kim, M.-S.; Karalkar, N. B.; Kim, H.-J.; Bates, A. M.; Watkins, N. E., Jr.; SantaLucia, H. A.; Meyer, A. J.; et al. Hachimoji DNA and RNA: A Genetic System with Eight Building Blocks. *Science* **2019**, *363*, 884−887.
(27) Huang, S. R.; Turećek, F. Cation Radicals of Hachimoji Nucleobases. Canonical Purine and Noncanonical Pyrimidine Forms Generated in the Gas Phase and Characterized by UV-Vis Photodissociation Action Spectroscopy. *J. Phys. Chem. A* **2020**, *124*, 7101−7112.
(28) Huang, S. R.; Turecek, F. Cation Radicals of Hachimoji Nucleobases P and Z: Generation in the Gas Phase and Characterization by UV-Vis Photodissociation Action Spectroscopy and Theory. *J. Am. Soc. Mass Spectrom.* **2021**, *32*, 373−386.
(29) Turećek, F. Flying DNA Cation Radicals in the Gas Phase: Generation and Action Spectroscopy of Canonical and Noncanonical Nucleobase Forms. *J. Phys. Chem. B* **2021**, *125*, 7090−7100.
(30) Liu, Y.; Dang, A.; Urban, J.; Tureček, F. Charge-Tagged DNA Radicals in the Gas Phase Characterized by UV-Vis Photodissociation Action Spectroscopy. *Angew. Chem., Int. Ed.* **2020**, *59*, 7772−7777.
(31) Korn, J. A.; Urban, J.; Dang, A.; Nguyen, H. T. H.; Turecek, F. UV-Vis Action Spectroscopy Reveals a Conformational Collapse in Hydrogen-Rich Dinucleotide Cation Radicals. *J. Phys. Chem. Lett.* **2017**, *8*, 4100−4107.
(32) Wan, J.; Brož, B.; Liu, Y.; Huang, S. R.; Marek, A.; Tureček, F. The DNA Radical Code. Resolution of Identity in Dissociations of Trinucleotide Cation Radicals in the Gas Phase. *J. Am. Soc. Mass Spectrom.* **2023**, *34*, 304−319.
(33) Liu, Y.; Huang, S. R.; Tureček, F. Guanine-Adenine Interactions in DNA Tetranucleotide Cation Radicals Revealed by UV/Vis Photodissociation Action Spectroscopy and Theory. *Phys. Chem. Chem. Phys.* **2020**, *22*, 16831−16842.
(34) Zima, V.; Liu, Y.; Tureček, F. Radical Cascade Dissociation Pathways to Unusual Nucleobase Cation Radicals. *J. Am. Soc. Mass Spectrom.* **2022**, *33*, 1038−1047.
(35) Chyall, L. J.; Kenttámaa, H. I. Gas-Phase Reactions of the 4-Dehydroanilinium Ion and Its Isomers. *J. Mass Spectrom.* **1995**, *30*, 81−87.
(36) Petzold, C. J.; Nelson, E. D.; Lardin, H. A.; Kenttámaa, H. I. Charge-Site Effects on the Radical Reactivity of Distonic Ions. *J. Phys. Chem. A* **2002**, *106*, 9767−9775.
(37) Widjaja, F.; Jin, Z.; Nash, J. J.; Kenttámaa, H. I. Comparison of the Reactivity of the Three Distonic Isomers of the Pyridine Radical Cation Toward Tetrahydrofuran in Solution and in the Gas Phase. *J. Am. Soc. Mass Spectrom.* **2013**, *24*, 469−480.
(38) Kotha, R. R.; Yerabolu, R.; Aqueel, M. S.; Riedeman, J. S.; Szalwinski, L.; Ding, D.; Nash, J. J.; Kenttámaa, H. I. Quinoline Triradicals: A Reactivity Study. *J. Am. Chem. Soc.* **2019**, *141*, 6672−6679.
(39) Ly, T.; Julian, R. R. Residue-Specific Radical-Directed Dissociation of Whole Proteins in the Gas Phase. *J. Am. Chem. Soc.* **2008**, *130*, 351−358.
(40) Liu, Z.; Julian, R. R. Deciphering the Peptide Iodination Code: Influence on Subsequent Gas-Phase Radical Generation with Photodissociation ESI-MS. *J. Am. Soc. Mass Spectrom.* **2009**, *20*, 965−971.
(41) Ly, T.; Julian, R. R. Tracking Radical Migration in Large Hydrogen Deficient Peptides with Covalent Labels: Facile Movement does not Equal Indiscriminate Fragmentation. *J. Am. Soc. Mass Spectrom.* **2009**, *20*, 1148−1158.
(42) Kazakbayeva, Z.; Zhumagali, S.; Mahboob, A.; O'Reilly, R. J. Homolytic C-Br Bond Dissociation Energies Obtained by Means of the G4 Thermochemical Protocol. *Chem. Data. Coll.* **2016**, *2*, 43−48.
(43) Blanksby, S. J.; Ellison, G. B. Bond Dissociation Energies of Organic Molecules. *Acc. Chem. Res.* **2003**, *36*, 255−263.
(44) Antoine, R.; Dugourd, P. UV-Visible Activation of Biomolecular Ions. In *Laser Photodissociation and Spectroscopy of Mass-Separated Biomolecular Ions*; Polfer, N. C., Dugourd, P., Eds.; Springer International Publishing: Cham, 2013; pp 93−116.
(45) Polfer, N. C., Dugourd, P., Eds. Laser Photodissociation and Spectroscopy of Mass Separated Biomolecular Ions. *Lecture Notes in Chemistry*; Springer: Cham, 2013; Vol. *83*, pp 13−20.
(46) Tureček, F. UV-Vis Spectroscopy of Gas-Phase Ions. *Mass Spectrom. Rev.* **2023**, *42*, 206−226.
(47) Marlton, S. J. P.; Trevitt, A. J. The Combination of Laser Photodissociation, Action Spectroscopy, and Mass Spectrometry to Identify and Separate Isomers. *Chem. Commun.* **2022**, *58*, 9451−9467.
(48) Huang, S. R.; Dang, A.; Tureček, F. Ground and Excited States of Gas-Phase DNA Nucleobase Cation-Radicals. A UV-Vis Photodissociation Action Spectroscopy and Computational Study of Adenine and 9-Methyladenine. *J. Am. Soc. Mass Spectrom.* **2020**, *31*, 1271−1281.
(49) Dang, A.; Liu, Y.; Turecek, F. UV-Vis Action Spectroscopy of Guanine, 9-Methylguanine and 2'-Deoxyguanosine Cation Radicals in the Gas Phase. *J. Phys. Chem. A* **2019**, *123*, 3272−3284.
(50) Lesslie, M.; Lawler, J. T.; Dang, A.; Korn, J. A.; Bím, D.; Steinmetz, V.; Maitre, P.; Turećek, F.; Ryzhov, V. Cytosine Radical Cation: a Gas-Phase Study Combining IRMPD Spectroscopy, UV-PD Spectroscopy, Ion−Molecule Reactions, and Theoretical Calculations. *ChemPhysChem* **2017**, *18*, 1293−1301.
(51) Dang, A.; Nguyen, H. T. H.; Ruiz, H.; Piacentino, E.; Ryzhov, V.; Tureček, F. Experimental Evidence for Non-Canonical Thymine Cation Radicals in the Gas Phase. *J. Phys. Chem. B* **2018**, *122*, 86−97.
(52) Giles, K.; Ujma, J.; Wildgoose, J.; Pringle, S.; Richardson, K.; Langridge, D.; Green, M. A Cyclic Ion Mobility-Mass Spectrometry System. *Anal. Chem.* **2019**, *91*, 8564−8573.
(53) Gozzo, T. A.; Bush, M. F. Effects of Charge on Protein Ion Structure: Lessons from Cation-to-Anion, Proton-Transfer Reactions. *Mass Spectrom. Rev.* **2023**, 1−26.
(54) Moss, C. L.; Chamot-Rooke, J.; Brown, J.; Campuzano, I.; Richardson, K.; Williams, J.; Bush, M.; Bythell, B.; Paizs, B.; Tureček, F. Assigning Structures to Gas-Phase Peptide Cations and Cation-Radicals. An Infrared Multiphoton Dissociation, Ion Mobility, Electron Transfer and Computational Study of a Histidine Peptide Ion. *J. Phys. Chem. B* **2012**, *116*, 3445−3456.
(55) Platt, S. P.; Attah, I. K.; Aziz, S.; El-Shall, S. Communication: Ion Mobility of the Radical Cation Dimers: $(Naphthalene)^{2+\bullet}$ and $Naphthalene^{+\bullet}$-Benzene: Evidence for Stacked Sandwich and T-shape Structures. *J. Chem. Phys.* **2015**, *142*, 191102.
(56) Adamson, B. D.; Coughlan, N. J. A.; Continetti, R. E.; Bieske, E. J. Changing the Shape of Molecular Ions: Photoisomerization Action Spectroscopy in the Gas Phase. *Phys. Chem. Chem. Phys.* **2013**, *15*, 9540−9548.
(57) Adamson, B. D.; Coughlan, N. J. A.; Markworth, P. B.; Continetti, R. E.; Bieske, E. J. An Ion Mobility Mass Spectrometer for Investigating Photoisomerization and Photodissociation of Molecular Ions. *Rev. Sci. Instrum.* **2014**, *85*, 123109.
(58) Dang, A.; Korn, J. A.; Gladden, J.; Mozzone, B.; Tureček, F. UV-Vis Photodissociation Action Spectroscopy on Thermo LTQ-XL ETD and Bruker amaZon Ion Trap Mass Spectrometers: A Practical Guide. *J. Am. Soc. Mass Spectrom.* **2019**, *30*, 1558−1564.


https://doi.org/10.1021/acs.jpca.3c03179
J. Phys. Chem. A 2023, 127, 5899−5913

(59) Becke, A. D. Density-Functional Exchange-Energy Approximation with Correct Asymptotic Behavior. *Phys. Rev. A* **1988**, *38*, 3098−3100.
(60) Zhao, Y.; Truhlar, D. G. The M06 Suite of Density Functionals for Main Group Thermochemistry, Thermochemical Kinetics, Noncovalent Interactions, Excited States, and Transition Elements: Two New Functionals and Systematic Testing of Four M06-Class Functionals and 12 Other Functionals. *Theor. Chem. Acc.* **2008**, *120*, 215−241.
(61) Møller, C.; Plesset, M. S. Note on the Approximation Treatment for Many-Electron Systems. *Phys. Rev.* **1934**, *46*, 618.
(62) Dunning, T. H., Jr. Gaussian Basis Sets for Use in Correlated Molecular Calculations. I. The Atoms Boron through Neon and Hydrogen. *J. Chem. Phys.* **1989**, *90*, 1007−1023.
(63) Halkier, A.; Helgaker, T.; Jørgensen, P.; Klopper, W.; Koch, H.; Olsen, J.; Wilson, A. K. Basis Set Convergence in Correlated Calculations on Ne, N2, and H2O. *Chem. Phys. Lett.* **1998**, *286*, 243−252.
(64) Helgaker, T.; Klopper, W.; Koch, H.; Noga, J. Basis-Set Convergence of Correlated Calculations on Water. *J. Chem. Phys.* **1997**, *106*, 9639−9646.
(65) Ćížek, J. On the Use of the Cluster Expansion and the Technique of Diagrams in Calculations of Correlation Effects in Atoms and Molecules. *Adv. Chem. Phys.* **2007**, *14*, 35−89.
(66) Purvis, G. D., III; Bartlett, R. J. Full Coupled-Cluster Singles and Doubles Model-the Inclusion of Disconnected Triples. *J. Chem. Phys.* **1982**, *76*, 1910−1918.
(67) Furche, F.; Ahlrichs, R. Adiabatic Time-Dependent Density Functional Methods for Excited State Properties. *J. Chem. Phys.* **2002**, *117*, 7433−7447.
(68) Wigner, E. On The Quantum Correction for Thermodynamic Equilibrium. *Phys. Rev.* **1932**, *40*, 749−759.
(69) Bonaćić-Koutecký, V.; Mitrić, R. Theoretical Exploration of Ultrafast Dynamics in Atomic Clusters: Analysis and Control. *Chem. Rev.* **2005**, *105*, 11−66.
(70) Barbatti, M.; Ruckenbauer, M.; Plasser, F.; Pittner, J.; Granucci, G.; Persico, M.; Lischka, H. Newton-X: A Surface-Hopping Program for Nonadiabatic Molecular Dynamics. *Wiley Interdisciplinary Reviews. Comput. Mol. Sci.* **2014**, *4*, 26−33.
(71) Mesleh, M. F.; Hunter, J. M.; Shvartsburg, A. A.; Schatz, G. C.; Jarrold, F. F. Structural Information from Ion Mobility Measurements: Effects of the Long Range Potential. *J. Phys. Chem.* **1996**, *100*, 16082−16086.
(72) Lee, J. W.; Davidson, K. L.; Bush, M. F.; Kim, H. I. Collision Cross Sections and Ion Structures: Development of a General Calculation Method via High-Quality Ion Mobility Measurements and Theoretical Modeling. *Analyst* **2017**, *142*, 4289−4298.
(73) Lee, J. W.; Lee, H. H.; Davidson, K. L.; Bush, M. F.; Kim, H. I. Structural Characterization of Small Molecular Ions by Ion Mobility Mass Spectrometry in Nitrogen Drift Gas: Improving the Accuracy of Trajectory Method Calculations. *Analyst* **2018**, *143*, 1786−1796.
(74) Zhu, L.; Hase, W. L. *Quantum Chemistry Program Exchange; Program no. QCPE 644*; Indiana University: Bloomington, IN, 1994.
(75) Gregersen, J. A.; Tureček, F. Mass-Spectrometric and Computational Study of Tryptophan Radicals (Trp + H)• Produced by Collisional Electron Transfer to Protonated Tryptophan in the Gas Phase. *Phys. Chem. Chem. Phys.* **2010**, *12*, 13434−13447.
(76) Turecek, F.; Chen, X. Protonated Adenine: Tautomers, Solvated Clusters, and Dissociation Mechanisms. *J. Am. Soc. Mass Spectrom.* **2005**, *16*, 1713−1726.
(77) Marian, C.; Nolting, D.; Weinkauf, R. The Electronic Spectrum of Protonated Adenine: Theory and Experiment. *Phys. Chem. Chem. Phys.* **2005**, *7*, 3306−3316.
(78) Cheong, N. R.; Nam, S. W.; Park, H. S.; Ryu, S.; Song, J. K.; Park, S. M.; Pérot, M.; Lucas, B.; Barat, M.; Fayeton, J. A.; Jouvet, C. Photofragmentation in Selected Tautomers of Protonated Adenine. *Phys. Chem. Chem. Phys.* **2011**, *13*, 291−295.
(79) Hud, N. V.; Morton, T. H. DFT Energy Surfaces for Aminopurine Homodimers and Their Conjugate Acid Ions. *J. Phys. Chem. A* **2007**, *111*, 3369−3377.
(80) Heldmaier, F. V.; Coughlan, N. J. A.; Haack, A.; Huard, R.; Guna, M.; Schneider, B. B.; Le Blanc, J. C.; Campbell, J. L.; Nooijen, M.; Hopkins, W. S. UVPD Spectroscopy of Differential Mobility-Selected Prototropic Isomers of Protonated Adenine. *Phys. Chem. Chem. Phys.* **2021**, *23*, 19892−19900.
(81) Huang, S. R.; Nováková, G.; Marek, A.; Tureček, F. The Elusive Non-Canonical Isomers of Ionized 9-Methyladenine and 2'-Deoxyadenosine. *J. Phys. Chem. A* **2021**, *125*, 338−348.
(82) Nelson, C. C.; McCloskey, J. A. Collision-Induced Dissociation of Adenine. *J. Am. Chem. Soc.* **1992**, *114*, 3661−3668.
(83) Chen, X.; Syrstad, E. A.; Gerbaux, P.; Nguyen, M. T.; Tureček, F. Distonic Isomers and Tautomers of Adenine Cation Radical in the Gas Phase and Aqueous Solution. *J. Phys. Chem. A* **2004**, *108*, 9283−9293.




https://doi.org/10.1021/acs.jpca.3c03179
J. Phys. Chem. A 2023, 127, 5899−5913